RSC Advances

PAPER

View Article Online
View Journal | View Issue

Cite this: *RSC Adv.*, 2025, **15**, 48816

Structural, thermodynamics, and mechanistic insights into a tobacco-waste derived activated carbon/polysaccharide composite sponge for efficient Cr(VI) adsorption and reusability

Ahlem Guesmi,[a] Naoufel Ben Hamadi,[a] Wesam Abd El-Fattah,[a] Mohamed A. El-Bindary,[b] Mohamed G. El-Desouky *[c] and Ashraf A. El-Bindary [d]

This study presents the creation of an innovative bioadsorbent a porous carbon–polymer composite, referred to as TACGC, was synthesized utilizing residues from tobacco processing and subsequently assessed for its efficacy as an adsorbent of hexavalent chromium (Cr(VI)) from aqueous solutions. The composite was fabricated by integrating tobacco-derived activated carbon into a matrix composed of guar gum and carboxymethyl cellulose, which was chemically cross-linked with itaconic acid, resulting in a stable and functional sponge-like structure. The structural and surface characteristics were investigated through various analytical techniques, including XRD, FT-IR, XPS, SEM–EDX, and BET analysis. These analyses collectively confirmed the development of a mesoporous network characterized by an abundance of oxygenated functional groups. Batch adsorption experiments indicated that factors such as pH, adsorbent dosage, initial Cr(VI) concentration, contact time, and temperature significantly impacted the removal efficiency. The observed adsorption behavior adhered to the Langmuir isotherm model, achieving a maximum adsorption capacity of 404.87 mg g^{-1}, while the kinetic data conformed to the pseudo-second-order model, suggesting that the uptake mechanism is predominantly chemisorption-driven. Thermodynamic analysis ($\Delta H°$ = 93.45 kJ mol^{-1}; $\Delta S°$ = 325.7 J mol^{-1} K^{-1}) established that the adsorption process is both spontaneous and endothermic. Moreover, TACGC demonstrated sustained efficiency over five cycles of adsorption–desorption, underscoring its structural integrity and reusability. The robustness of the system was further corroborated through statistical optimization employing the Box–Behnken design. These results underscore the significant potential of TACGC as an effective and sustainable solution for Cr(VI) remediation in wastewater treatment contexts.

Received 26th September 2025
Accepted 2nd December 2025

DOI: 10.1039/d5ra07331f

rsc.li/rsc-advances

1. Introduction

The issue of environmental pollution attributed to heavy metals has emerged as a significant global challenge, primarily driven by elements that include swift industrial development, the expansion of urban areas, and various human activities. Among various heavy metals, hexavalent chromium (Cr(VI)) stands out as particularly dangerous due to its high solubility, mobility, and serious carcinogenic, mutagenic, and teratogenic impacts on living organisms. Cr(VI) is widely utilized in several industrial operations, including electroplating, leather tanning, textile dyeing, and pigment production.[1] If the wastewater generated from these processes is not properly treated, it can lead to contamination of surface and groundwater, presenting noteworthy hazards to human health and ecosystems. Therefore, the development of effective and sustainable technologies aimed at extracting Cr(VI) from aquatic systems has become a significant area of emphasis within the fields of environmental science and engineering. Conventional techniques employed for the elimination of heavy metals encompass various approaches like as membrane filtration, chemical precipitation, ion exchange, electrochemical methods, reverse osmosis, and coagulation–flocculation. Although these methods can be effective in controlled settings, they frequently face considerable disadvantages such as high operational costs, complicated infrastructure, secondary waste production, and limited effectiveness at low concentrations of metals. In this context, adsorption has emerged as a viable alternative, noted for its simplicity, cost efficiency, operational versatility, and potential for regenerating the adsorbent. The effectiveness of adsorption

[a]*Chemistry Department, College of Science, Imam Mohammad Ibn Saud Islamic University (IMSIU), P. O. Box 5701, Riyadh 11432, Saudi Arabia*

[b]*Basic Science Department, Higher Institute of Engineering and Technology, New Damietta 34517, Egypt*

[c]*Egyptian Propylene and Polypropylene Company, Port Said 42511, Egypt. E-mail: ch.moh.gamal@gmail.com*

[d]*Chemical Department, Faculty of Science, Damietta University, Damietta 34517, Egypt*

methods is profoundly precious by the physicochemical appearances of the adsorbent material. Key factors to consider include the surface area, porosity, attendance of useful groups, and the mechanical stability of the material.[2]

Tobacco processing remains a substantial agro-industrial sector worldwide, and despite the gradual decline in smoking rates due to global public health campaigns, tobacco agriculture and manufacturing continue to generate large quantities of lignocellulosic waste.[3] This waste originates primarily from farming and industrial operations such as curing, sorting, cutting, nicotine extraction, and cigarette manufacturing rather than from consumer use. Consequently, significant volumes of stems, midribs, dust, rejected leaves, and production offcuts are produced annually, representing 20–30% of the total harvested biomass. These residues are typically discarded or burned, contributing to environmental pollution. Owing to their high carbon content, inherent porosity, and abundance of oxygen- and nitrogen-containing functional groups, tobacco byproducts serve as an excellent low-cost precursor for preparing activated carbon-based adsorbents.[4] Valorizing this abundant waste stream not only supports circular-economy strategies and reduces disposal burdens, but also enables the development of efficient and sustainable materials for heavy-metal removal from wastewater. Therefore, the use of tobacco-derived waste as an adsorbent precursor is both environmentally justified and technologically advantageous.[5]

In current years, there has been a heightened importance on the development of economical, sustainable, and effective bioadsorbents derived from agricultural and industrial byproducts.[6] These bioadsorbents not only offer an economical approach for the remediation of heavy metals but also assist in waste valorization and promote circular economy initiatives. One notable type of biomass is tobacco waste, which is a plentiful but often overlooked byproduct of the tobacco industry. This waste is characterized by its high carbon content and natural fibrous structure, enabling its thermal conversion into activated carbon with desirable textural attributes.[7] Tobacco-derived activated carbon (TAC) exhibits significant porosity and a large surface area, alongside oxygenated functional groups on its surface. These characteristics contribute to its efficacy as a potent adsorbent for heavy metal ions. Nonetheless, standard activated carbon can have drawbacks, including issues with particle clumping, diminished mechanical stability in water, and difficulties in recovery after use. To mitigate these challenges, researchers have investigated the possibility of encapsulating activated carbon within biopolymer matrices, resulting in composite materials with improved handling characteristics and enhanced adsorption capabilities. Biopolymers such as guar gum (GG) and carboxymethyl cellulose (CMC) are frequently utilized in environmental applications due to their biodegradability, hydrophilicity, and a rich variety of functional groups that can bond with heavy metal ions.[8,9] Guar gum, a naturally occurring galactomannan polysaccharide, is renowned for its remarkable viscosity-regulating and gel-forming attributes, while carboxymethyl cellulose, a derivative of cellulose containing carboxyl functional groups, improves water solubility and metal binding efficiency.[10]

The process of crosslinking these polymers using a biocompatible agent such as itaconic acid (IA) facilitates the formation of a three-dimensional polymeric network. This structural transformation not only bolsters the integrity of the material but also augments the density of functional groups present within the hydrogel composite. Itaconic acid, a renewable dicarboxylic acid obtained through fermentation, presents multiple potential sites for esterification and ionic interactions with metal ions.[11] When coupled with TAC, the GG–CMC hydrogel network crosslinked with IA forms a stable and highly functional composite known as TACGC.[12] This composite effectively utilizes the adsorptive characteristics of activated carbon alongside the ion exchange attributes of the polymer matrix, facilitating a synergistic approach for the remediation of Cr(VI). To comprehensively evaluate the efficacy of the TACGC composite in Cr(VI) adsorption, a sequence of batch tests were conducted to examine the effect of crucial operational limits, including pH, adsorbent amount, original metal concentration, communication time, and temperature.[13] The obtained adsorption data were analyzed through the application of multiple isotherm models, specifically the models of Langmuir as well as Freundlich, to elucidate the nature of the adsorption procedure.[14] The Langmuir isotherm suggests that adsorption occurs as a monolayer on a unvarying surface, while the Freundlich model illustrates the adsorption phenomenon on surfaces that are heterogeneous, reflecting a range of affinities. Additionally, kinetic models, namely pseudo-first-order and pseudo-second-order, were employed to analyze the adsorption rate and elucidate the underlying mechanism. The pseudo-second-order model posits that the rate-limiting step in the adsorption development is chemisorption. This model demonstrated the critical nature of interactions marked by valence forces and the transfer of electrons between the adsorbent and Cr(VI) ions by offering a better fit to the experimental results.[15]

An analysis of thermodynamic parameters was conducted to gain insights into the spontaneity, feasibility, and thermal interactions pertinent to the adsorption procedure. The positive ΔH° value signifies that the adsorption of Cr(VI) onto the TACGC material occurs as an endothermic process. Conversely, the negative ΔG° values substantiate the spontaneous nature of this reaction. Furthermore, the positive ΔS° value indicates an increase in disorder at the solid–liquid interface during the adsorption process, most likely as a result of water molecules being displaced by Cr(VI) ions on the adsorbent's surface.[16] The TACGC composite's ability to regenerate and reuse *via* numerous cycles of adsorption and desorption was examined in order to assess its practical usefulness.[16] Notably, the composite maintained substantial efficiency in removing Cr(VI) up to the fifth cycle, highlighting its potential for repeated application in real-world scenarios. The desorption process utilized mild eluting agents, and the structural integrity of the composite was largely preserved, reinforcing its stability and reusability.[17]

The study used a statistical experimental framework known as the Box–Behnken design (BBD) to maximize the adsorption process and boost the efficacy of Cr(VI) removal. This approach, classified as a response surface methodology, allows for the

simultaneous examination of multiple variables along with their interactions.[18] The application of BBD effectively decreases the number of necessary tests, while concurrently attractive the robustness of the resultant model. This strategic approach enabled the identification of the ideal operating conditions that yield the highest adsorption capacity, thereby offering a predictive framework suitable for the upscaling of the process in industrial settings.[19]

This study presents an innovative and eco-friendly adsorbent developed through the integration of activated carbon sourced from tobacco waste into a biopolymer framework that includes guar gum (GG) and carboxymethyl cellulose (CMC), which has been crosslinked using itaconic acid (IA). The research highlights the innovative utilization of agricultural tobacco waste to produce a functional and sustainable adsorbent, marking the first instance of combining TAC with a GG-CMC hydrogel network that is stabilized by (IA). This hybrid adsorbent demonstrates enhanced efficacy in the extraction of Cr(VI), attributable to its substantial surface area and an abundance of functional groups (–OH, –COOH). These properties promote both electrostatic interactions and redox processes, thereby optimizing its performance. The study includes a thorough analysis of the adsorption characteristics, employing kinetic, isotherm, and thermodynamic modeling to demonstrate a mechanism that is spontaneous and endothermic. Furthermore, the composite material showed exceptional reusability across five cycles and underwent statistical optimization *via* Box–Behnken Design, which enhances performance while reducing the need for extensive experimentation. This method offers an economical and scalable solution for water purification and the valorization of waste biomass.

2. Experimental

Table S1 lists the chemicals in detail, while Table S2 gives a comprehensive rundown of all the instruments used.

2.1. Synthesis of adsorbent

2.1.1. Synthesis of disposable burned tobacco activated carbon (TAC). The used tobacco from disposable products underwent a treatment process involving a saturated potassium hydroxide (KOH) solution, applied at a mass ratio of 1 : 1 relative to the disposable masks. This treatment occurred over three hours under ambient temperature conditions. After the impregnation procedure, the processed material was subjected to a drying step within a laboratory oven for 19 hours, during which a consistent temperature of 150 °C was upheld. After the drying phase, the material proceeded to undergo carbonization in a furnace at a specified temperature of 650 °C in the absence of oxygen (to prevent of combustion of the biomass and to allow proper activation). In the subsequent phase, the carbonized product underwent a washing process utilizing distilled water, specifically designed to eliminate any residual KOH, until a neutral pH was attained. Following this procedure, the samples were exposed to a treatment with 1 M HCl, after which they were washed once more until achieving a neutral pH. Ultimately, the resultant carbon-based material was subjected to a drying process at 150 °C for a duration of 12 hours.[20]

2.1.2. Synthesis of TACGC. Guar gum (GG) and carboxymethylcellulose (CMC) crosslinked with itaconic acid (IA) form a novel bio-based composite designed to improve environmental remediation processes and facilitate controlled release applications. The synthesis of (TACGC) begins by dispersing approximately 1.0 g of tobacco activated carbon (TAC) in 50 mL distilled water through ultrasonication, ensuring uniform particle distribution. Concurrently, GG and CMC are dissolved in distilled water at concentrations ranging from 1% to 2% (w/v) each, creating a homogeneous, viscous polymer mixture while maintaining constant stirring at temperatures between 60 and 70 °C. Itaconic acid, a bi-functional unsaturated dicarboxylic acid, is introduced into the mixture at a concentration of about 5% to 10% (w/w, based on total polymer weight), serving as the crosslinking agent. The pH is adjusted to approximately 4 to 5 to foster esterification and ionic interactions.[21] Subsequently, the activated carbon dispersion is added incrementally to the GG-CMC-IA mixture, and heating to 80 °C is applied to trigger *in situ* crosslinking and encapsulation. The final gel can be molded into beads or films and is then dried at 50 °C. This encapsulated composite leverages the hydrophilic and biodegradable attributes of GG and CMC, while also utilizing the pH-sensitive and ionically interactive features of itaconic acid. Additionally, it benefits from the amplified surface area and adsorption potential offered by activated carbon (Fig. 1).

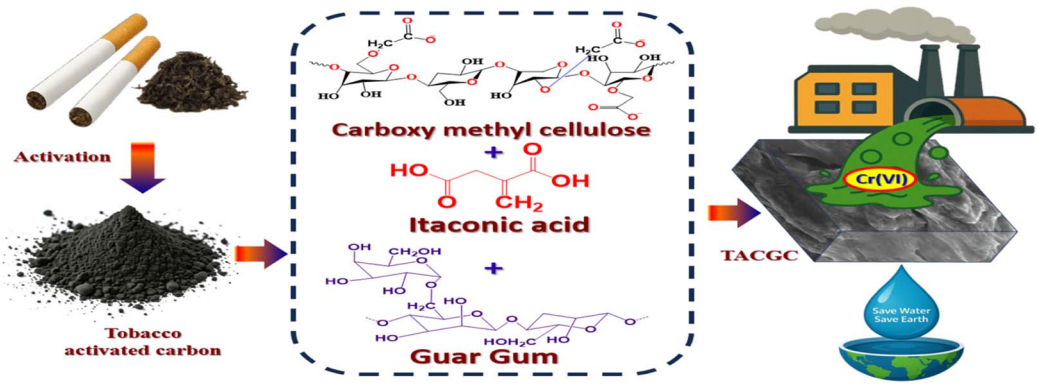

Fig. 1 Representation illustration of synthesis of TACGC composite sponge.

2.2. Removal and batch studies of the Cr(VI) *via* TACGC

A complete study was directed to assess the adsorption capacity of the TACGC, emphasizing factors counting pH, dosage, concentration, time, and temperature. Within a regulated batch system with a whole volume of 25 mL, the adsorption process for Cr(VI) was examined over a concentration from 40 to 480 mg L^{-1}.[22] The pH planes were systematically attuned in the range of 2 to 8, and the length of contact was modified between 5 to 100 min. Furthermore, the research thoroughly investigated the influence of various quantities of adsorbents, spanning from 0.02 to 0.5 g, in conjunction with temperature variations reaching from 20 to 45 °C. In order to regulate the pH levels, 0.1 N of HCl and/or NaOH were employed as regulating agents, as depicted in Fig. 2. The data obtained from these adjustments was subsequently analyzed to examine isotherms, kinetic behavior, and the temperature effect on the thermodynamic belongings related with the adsorption process. The evaluation of the research samples was conducted using flame atomic absorption spectrometer. Each sample's sorption capabilities were calculated by averaging the outcomes of three different tests.[23] As a result, the amount of absorbed Cr(VI), designated as q_e, was determined alongside the removal percentage (%RE), employing eqn (1) and (2) for these calculations, respectively.

$$q_e = \frac{(C_i - C_t)V}{M} \quad (1)$$

$$\%R = \frac{(C_i - C_t)}{C_i} \times 100 \quad (2)$$

2.3. Design of experiments

The Response Surface Methodology (RSM) represents a comprehensive approach for developing intricate statistical models within environments that present a variety of possible results. Clarifying the relationships between the response variable and the different settings involved is its primary goal. Additionally, using these statistical models helps to improve the techniques that are being studied. In order to evaluate each sample, the sorption capacities were determined by averaging the results of three different experimental trials. The removal percentage (%RE) as well as the total quantity of Cr(VI) adsorbed (q_e) were calculated using eqn (1) and (2). An organized approach that methodically conducts a number of well-planned studies is called Response Surface Methodology (RSM). This methodology focuses on the essential elements of the process to systematically seek out the most effective solution within a comprehensive operational context. Central Composite Design (CCD) serves as a prevalent technique for optimizing process limits. Eqn (1) delineates the quantity of Cr(VI) absorbed per g of the adsorbent over distinct time intermissions (t), with a particular emphasis on the TACGC composite sponge as the material used for adsorption. Moreover, eqn (2) establishes a systematic approach for assessing the efficacy of the removal process. The analysis highlighted three critical variables impacting this process: "mass of adsorbent", "communication time", and "solution pH". These variables were designated for investigation based on their demonstrated adverse effects on the adsorption capability (Table S3).[24]

Three essential elements make up the central composite design: determining the model coefficients, creating the experimental framework, and forecasting the model's outcomes. A thorough and comprehensive analysis of the resulting data is required for each phase. After completing these preparatory steps, a methodical empirical model is produced, which makes it possible to evaluate how the function behaves in relation to various input variable pairings. Therefore, a model of quadratic regression is established, as outlined in eqn (3):

$$Y = \beta_o + \sum\beta_i X_i + \sum\beta_{ii} X_i^2 + \sum\sum\beta_{ij} X_i X_j \quad (3)$$

In this analytical framework, the resistance coefficient is denoted by the symbol "i", while the speed coefficient is indicated by "j". The notation β_0, β_i, β_{ii}, and β_{ij} corresponds to various coefficients that pertain to resistance, interaction, speed, and the constant term, respectively. The metrics R^2, R_{Adj}^2, and R_{Pred}^2 were utilized to assess the performance of the proposed polynomial model equation.

The symbols "i" and "j" in this mathematical framework stand for the resistance and speed coefficients, respectively. Different coefficients related to resistance, connection, velocity, and the constant term are denoted by the notations β_0, β_i, β_{ii}, and β_{ij}, respectively. The performance of the suggested

Fig. 2 Diagrammatic representation of Cr(VI) adsorption and elimination onto TACGC.

polynomial model equation was evaluated using the metrics R^2, R_{Adj}^2, and R_{Pred}^2. A higher R^2 value implies enhanced prediction accuracy, suggesting a more vigorous relationship among the model and the actual investigational data.

The Box–Behnken design (BBD), as demonstrated in Table 1, is utilized to systematically evaluate the impacts of three pivotal factors pH, contact duration, and adsorbent quantity on the effectiveness of Cr(VI) adsorption by the synthesized TACGC composite sponge. Seventeen experimental trials were executed, each incorporating varied combinations of the specified variables. The resulting Cr(VI) adsorption yields, quantified in mg g^{-1}, were meticulously recorded alongside the expected results and any remaining residual values. The analysis designates that the peak adsorption capacity occurred at a pH level of 5, with an optimal contact length of 100 min and a minimal adsorbent dosage of 0.02 g (Run 2), which yielded a substantial result of 404.78 mg g^{-1}. This finding highlights the significance of moderately acidic conditions, as they contribute to enhanced adsorption efficiency, particularly when combined with extended contact times and reduced adsorbent quantities. Conversely, the data reveals that the lowest removal efficiency was recorded at a pH of 2, in conjunction with a mere 5 min of contact time and a higher adsorbent amount of 0.26 g (Run 8). This outcome underscores the negative impact of low pH levels and insufficient interaction periods on adsorption performance. Central experimental points, such as Runs 4, 7, 10, 14, and 15, consistently produced yields around 404.78 mg g^{-1} with minimal residuals, demonstrating the model's reliability and robustness. Although most residual values were low, some trials (specifically Runs 1, 2, 5, 8, 11, and 17) exhibited larger deviations, which may be attributed to non-linear interactions or variability in the experimental setup. The BBD model successfully illuminated the interactions among variables, demonstrating its utility in refining adsorption parameters and predicting system behavior. This reinforces the capability of the TACGC composite to serve as a versatile and efficient adsorbent for the remediation of Cr(VI), as outlined in Table 1.

Table 1 The absorption capabilities and surface interactions of the TACGC within the central composite structure necessitate thorough analysis and inspection

	Definite variables			Yield (mg g^{-1})		
Run	pH	Time (min)	Dose (g)	Investigational	Predicted	Residue
1	8	100	0.26	279.207	296.17	−16.96
2	5	100	0.02	404.85	384.95	19.90
3	5	100	0.5	253.031	239.21	13.82
4	5	52.5	0.26	287.806	287.81	0.0001
5	5	5	0.5	50.96	70.86	−19.90
6	8	52.5	0.02	299.319	302.26	−2.94
7	5	52.5	0.26	287.806	287.81	0.0001
8	2	5	0.26	42.25	25.29	16.96
9	2	52.5	0.02	233.843	236.98	−3.14
10	5	52.5	0.26	287.806	287.81	0.0001
11	8	5	0.26	56.2369	39.48	16.76
12	5	5	0.02	81.5435	95.36	−13.82
13	8	52.5	0.5	196.92	193.78	3.14
14	5	52.5	0.26	287.806	287.81	−0.0003
15	5	52.5	0.26	287.806	287.81	0.0001
16	2	52.5	0.5	178.166	175.23	2.94
17	2	100	0.26	209.767	226.53	−16.76

3. Results and discussion

3.1. Classification of TACGC composite sponge

3.1.1. X-ray diffraction (XRD). The X-ray diffraction (XRD) pattern of TACGC reveals a broad diffraction peak centered around 2θ = 25–30°. This peak is indicative of amorphous carbon structures typically found in activated carbons derived from biomass.[25] The presence of this broad hump suggests that the material consists of disordered, turbostratic carbon layers, highlighting its predominantly non-crystalline characteristics. Additionally, a sharper, more pronounced peak observed between 2θ = 32–35° may signify the existence of minor crystalline phases, which could originate from residual inorganic or from structural organization induced by interactions between the activated carbon and the encapsulating biopolymers. The intensity of the XRD pattern decreases gradually, with minor fluctuations detected between 40° and 70°, further supporting the notion of heterogeneity and the amorphous composition of the composite.[26] Furthermore, the encapsulation with guar gum and carboxymethyl cellulose not only contributes to the stabilization of the carbon structure but may also facilitate some degree of ordering due to polymer cross-linking. In summary, the XRD pattern validates the effective development of an amorphous carbon matrix encapsulated by polymers, which is suitable for adsorption and various functional applications (Fig. 3(a)).

3.1.2. N_2 adsorption–desorption isotherm. The nitrogen adsorption–desorption isotherms for both TACGC and Cr@TACGC, as represented in Fig. 3(b), fall into the category of Type IV isotherms, exhibiting H3-type hysteresis loops. This classification confirms their mesoporous nature. TACGC demonstrates a higher nitrogen uptake of approximately 240 cm^3 g^{-1}, suggesting a greater specific surface area and pore volume. In contrast, Cr@TACGC shows a reduced nitrogen uptake of around 150 cm^3 g^{-1}, indicating considerable pore blockage or surface coverage as a result of Cr(VI) adsorption. This analysis is supported by the BJH pore size distribution illustrated in Fig. 3(c). Here, TACGC displays a marked peak at around 1.2 nm. In contrast, Cr@TACGC shows a reduced peak intensity and a slight shift to a larger radius, approximately 1.5 nm. This change indicates alterations in structure and suggests partial obstruction of the pores.[27,28] The pore width distribution shown in Fig. 3(d) further reinforces this, as it indicates a marked decrease in intensity for Cr@TACGC, which points to a reduction in the availability of mesopores. Upon examining the information quantitatively, it is observed that the BET surface area experienced a reduction from 110.182 m^2 g^{-1} for TACGC to 90.0928 m^2 g^{-1} for Cr@TACGC. Concurrently, the average pore radius exhibited an increase from 12.38 to 15.14 nm. Additionally, there was a significant decline in the total pore volume, which decreased from 0.3308 to 0.126 cm^3 g^{-1}. The consequences indicate that the adsorption of Cr(VI) has resulted in a notable reduction in the available

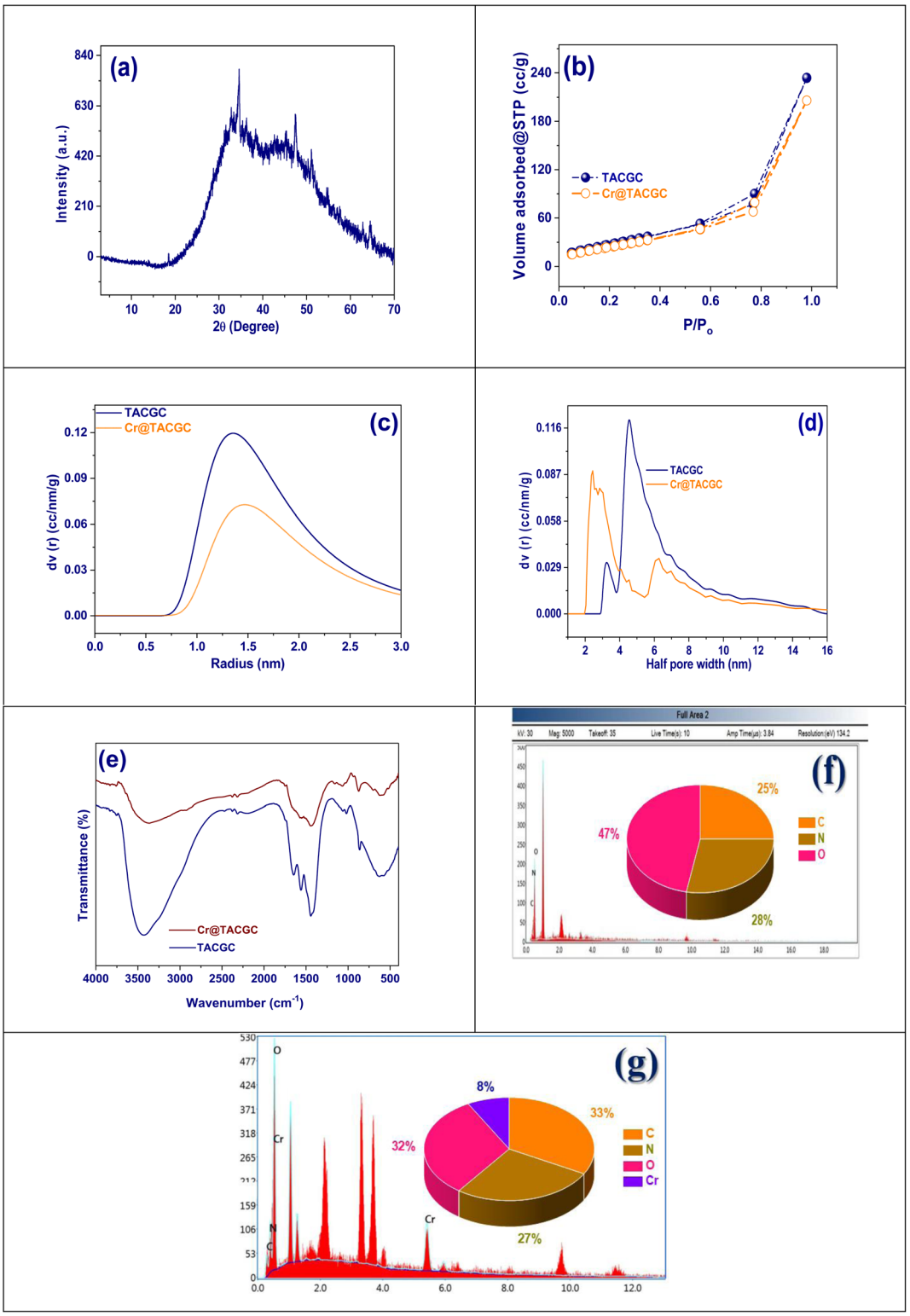

Fig. 3 (a) XRD pattern of TACGC, (b) N_2 adsorption–desorption isotherm of TACGC and Cr@TACGC, (c) pore radius distribution, (d) pore size distribution, (e) FT-IR of TACGC and Cr@TACGC, (f) EDX analysis of TACGC, and (g) EDX analysis of Cr@TACGC.

surface area and the integrity of the pore structure. This decline can be attributed to mechanisms such as pore filling and the adsorption occurring on internal surfaces.

3.1.3. FT-IR. The FT-IR spectra provide a detailed examination of the structural and functional changes occurring in TACGC and Cr@TACGC (post-chromium adsorption). These alterations indicate a significant interaction with metal ions.[29]

The observed spectra exhibit a pronounced band within the 3300–3400 cm^{-1} range, which is correlated with O–H stretching vibrations. These vibrations arise from hydroxyl groups present in the polysaccharide matrix, in calculation to aids from water molecules that are adsorbed on the surface. A reduction or shift in this band for Cr@TACGC suggests that hydroxyl groups are participating in chromium binding. Furthermore, the observed peak near 2900 cm^{-1} is indicative of C–H stretching within the organic matrix, thereby validating the inclusion of gum guar and carboxymethylcellulose. A distinct band observed around 1700–1730 cm^{-1} indicates C=O stretching from carboxylic or ester groups; this band experiences a slight shift in Cr@TACGC, which indicates possible coordination with chromium ions. The observed peaks in the range of 1600–1450 cm^{-1} resemble to both asymmetric as well as symmetric vibrations of COO^{-} groups. The variations noted in Cr@TACGC further substantiate the presence of metal–ligand interactions. In the 1000–1200 cm^{-1} range, related to C–O–C stretching in ether linkages, a decrease in intensity is noted after chromium adsorption, suggesting a structural rearrangement has occurred.[30,31] Lastly, additional variations or new bands appearing below 600 cm^{-1} may be indicative of Cr–O bonding, further confirming the successful immobilization of chromium onto the TACGC matrix. The experimental spectral alterations communally specify that TACGC contains functional groups that can efficiently bind chromium ions. This observation underscores its prospective utility as a biosorbent for the decontamination of heavy metals, as illustrated in Fig. 3(e).

3.1.4. EDX analysis. The Energy Dispersive X-ray (EDX) spectrum of TACGC reveals a specific elemental composition, consisting of 47% oxygen, 28% nitrogen, and 25% carbon. This composition validates the successful creation of a functionalized biocomposite. The notable oxygen concentration suggests a predominance of oxygenated functional groups, including hydroxyl, carboxyl, and carbonyl. This is primarily credited to the attendance of encapsulants like guar gum and carboxymethyl cellulose.[32] These groups show a critical character in increasing the hydrophilic nature of the material as well as its ability to adsorb metal ions. The presence of nitrogen indicates that nitrogen-containing functional groups might be derived either from the original tobacco source or from the chemical treatments applied during the preparation process. This enhancement likely contributes to the material's improved potential for forming coordination complexes with metal ions. The carbon element serves as the activated carbon nucleus, offering vital structural stability, an extensive surface area, and significant porosity, all of which are vital for efficient adsorption. The analysis of its elemental distribution indicates that TACGC possesses a chemically varied and reactive surface, thus establishing it as a viable candidate for environmental removal efforts, especially in the extraction of metal pollutants, as demonstrated in Fig. 3(f).

The EDX analysis of Cr@TACGC, which is tobacco-activated carbon that has been encapsulated with guar gum and carboxymethylcellulose after chromium adsorption, indicates a clear elemental composition. This material is comprised of 33% carbon, 32% oxygen, 27% nitrogen, and 8% chromium, indicating that chromium ions have successfully attached to the exterior of the composite structure. The high carbon content can be credited to both the activated carbon matrix and the polysaccharide encapsulants, which create a porous and stable structure necessary for adsorption processes.[33] The increased levels of oxygen suggest the attendance of various oxygenated practical groups, like as carboxyl, hydroxyl, and carbonyl. These groups predominantly play a character in attractive electrostatic interactions and forming complexes with metal ions. The substantial presence of nitrogen proposes the incorporation of nitrogenous groups, probable derived from the tobacco component or through polymer modifications, which further improve the material's capability to chelate heavy metals, such as chromium.[34] Crucially, the 8% chromium present, along with specific peaks in the spectrum, serves as direct evidence of effective chromium adsorption, confirming the functional capacity of the reactive sites within the TACGC framework. In summary, the results from the EDX analysis indicate that Cr@TACGC functions as a chemically active and versatile biosorbent. This material demonstrates significant promise for environmental applications, especially in the removal of toxic heavy metals from contaminated water foundations, as evidenced by the data presented in Fig. 3(g).

3.1.5. SEM analysis. Fig. 4(a–c) illustrate the surface topography of TACGC using various rendering techniques to improve the interpretation of its surface characteristics. Fig. 4(a) employs a grayscale height map that showcases the variations in surface roughness and elevation, drawing attention to the irregular and porous morphology typical of activated carbon-based materials. In Fig. 4(b), a thermal color gradient is used, with brighter hues like yellow and red representing higher elevations, thereby enhancing visual contrast and underscoring the material's significant surface roughness and intricate texture. Fig. 4(c) utilizes a deep blue color palette to depict the same topographic features, while placing greater emphasis on depth and shading, providing a different viewpoint of the surface profile. Despite the distinct color mappings, all three illustrations affirm the existence of a rugged and porous surface, which is crucial for the material's extensive surface area and prospective adsorption capabilities in environmental contexts.

Fig. 4(d) illustrates the results of scanning electron microscopy (SEM) alongside elemental mapping analysis of TACGC. This analysis highlights the structural characteristics and elemental constituents of the composite before it undergoes metal adsorption. The central SEM image depicts a rough, layered, and porous structure typical of bio-derived activated carbon materials, characterized by prominent surface folds and cavities that enhance surface area and adsorption capabilities. This morphology indicates the effective incorporation of the biopolymer matrix with the activated carbon, resulting in a stable and complex textural material. The elemental maps in proximity offer a comprehensive depiction of the spatial arrangement of key elements: oxygen (52%), nitrogen (26%), and carbon (22%). The significant dominance of oxygen indicates a concentrated occurrence of oxygen-comprising useful groups, such as hydroxyl (–OH), carbonyl (C=O), and carboxyl

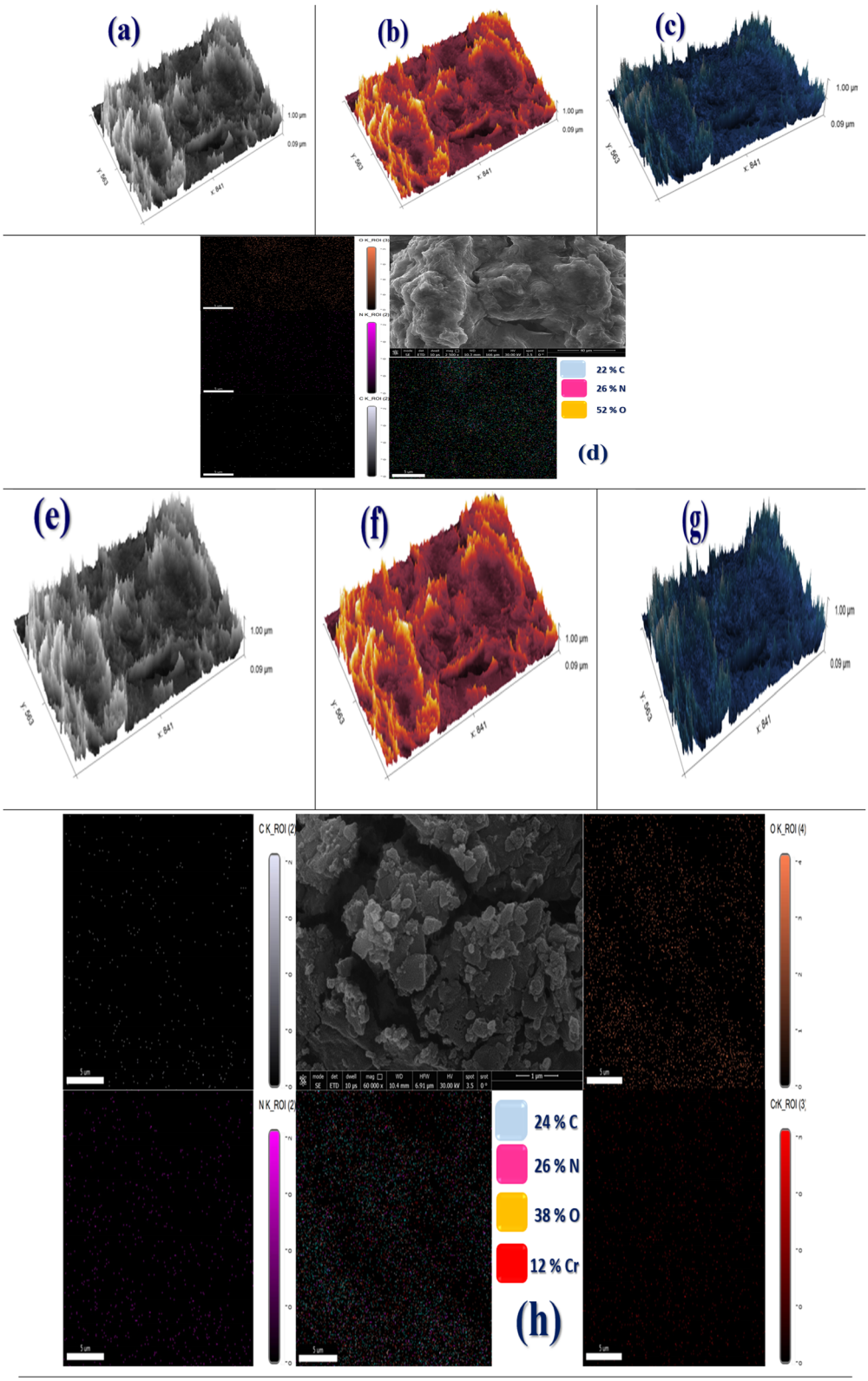

Fig. 4 FESEM images for TACGC and Cr@TACGC: (a) grayscale of TACGC, (b) thermal color of TACGC, (c) cool blue tones of TACGC, (d) SEM mapping of TACGC (e) grayscale of Cr@TACGC, (f) thermal color of Cr@TACGC, (g) cool blue tones of Cr@TACGC, (h) SEM mapping of Cr@TACGC.

(–COOH). These practical groups are largely contributed by the substances gum guar and carboxymethylcellulose. The uniform distribution of nitrogen indicates the presence of nitrogenous functionalities that may improve chemical reactivity and the potential for metal binding. Carbon serves as the core framework, ensuring structural integrity and contributing to the porous network.[35] The elemental maps' overlays reveal an unvarying distribution of the three elements during the material's surface, which validates the effectiveness of the encapsulation and functionalization processes employed. In conclusion, the data gained from SEM and EDX mapping corroborate the successful synthesis of TACGC, distinguished by its chemically active porous structure, which is well-suited for requests in adsorption and environmental cleanup.

Fig. 4(e–g) present the surface topography of the TACGC sample through different rendering techniques to enhance the understanding of its surface features. In Fig. 4(e), rendered in grayscale, the surface height distribution is clearly illustrated, drawing attention to the composite's structural irregularities and porosity. Fig. 4(f) employs a thermal color scheme, with bright yellow and red representing elevated areas, while darker tones correspond to lower regions, effectively highlighting the surface roughness and locations for adsorption. Meanwhile, Fig. 4(g) utilizes cool blue tones to provide a depth-focused perspective of the same surface, which underscores the differences in texture and topography. Although the color schemes differ, all three images refer to the same Cr@TACGC sample and indicate a slightly smoother surface morphology when compared to the unmodified TACGC. This observation suggests that some surface pores may be partially filled or covered due to effective Cr(VI) adsorption. The findings affirm the material's strong affinity for chromium ions, supporting its potential for environmental remediation applications.

The SEM and elemental mapping study of Cr@TACGC demonstrate a highly developed porous and rough surface morphology, typical of materials derived from activated carbon. The examined structure exhibits both fine and stratified characteristics, which contribute to a considerable surface area advantageous for processes related to adsorption. The analysis of the elemental distribution maps reveals a uniform presence of the elements: carbon (24%), nitrogen (26%), oxygen (38%), and chromium (12%) across the entirety of the composite material.[36] The carbon content originates from tobacco-based activated carbon and biopolymer encapsulants, which provide the composite's structural framework. In contrast, the nitrogen and oxygen are sourced from functional groups found in materials such as gum guar and carboxymethylcellulose, including amines, hydroxyls, and carboxyls, which enhance the chemical activity and capacity for metal binding of the material. The elemental mapping reveals a significant concentration and uniform dispersion of chromium, supporting the notion that Cr ions are effectively adsorbed on the surface of the TACGC matrix. This combination of a porous structure and evenly distributed functional components supports the characterization of Cr@TACGC as a chemically reactive and structurally stable biosorbent, making it particularly promising for environmental remediation efforts aimed at removing heavy metal contaminants from water sources Fig. 4(h).

3.1.6. XPS. The X-ray photoelectron spectroscopy (XPS) C 1s spectra for TACGC and Cr@TACGC provide valuable insights into the surface chemical states of carbon, highlighting their relevance to the adsorption characteristics of chromium. For TACGC, the deconvolution of the C 1s peaks reveals a prominent feature at 284.75 eV (68.83%), attributable to C–C/C=C bonds associated with the graphitic carbon framework. A peak observed at 286.16 eV (11.76%) has been identified as indicative of C–O bonds, which are likely derived from hydroxyl or ether functional groups present in guar gum and carboxymethyl cellulose (CMC). Additionally, a second peak located at 288.2 eV (19.86%) corresponds to O–C=O functional groups, specifically carboxylic or ester groups that play a vital character in the binding of metal ions. Post chromium adsorption in the Cr@TACGC system, there is a notable small shift in the C–C/C=C peak to 284.7 eV (67.15%). Concurrently, the C–O peak is displaced to 285.97 eV, with an increased contribution of 17.42%. In contrast, the O–C=O peak displays a shift to 288.47 eV, accompanied by a reduction in intensity to 15.43%. The observed changes in binding energies and the variations in relative peak strengths indicate that oxygen-covering practical groups, especially hydroxyl and carboxyl groups. This interaction may occur through mechanisms such as electron donation or surface complexation.[37] The reliability of the C–C peak suggests that the carbon backbone preserves its structural stability. In contrast, the variations noted in the C–O and O–C=O peaks corroborate the chemical connections occurring among chromium and the functionalized surface. Overall, the findings from the XPS analysis underline the critical character of surface functionalities in the adsorption mechanism. This supports the characterization of Cr@TACGC as a potent and reactive biosorbent for heavy metal remediation, as depicted in Fig. 5.

The XPS N 1s spectra gained for TACGC and Cr@TACGC provide significant information regarding the chemical states of nitrogen and their involvement in the adsorption process of chromium. Within TACGC, the primary N 1s peak appears at 399.03 eV (93.34%), indicative of pyrrolic or amine-like nitrogen species (–NH or $-NH_2$). A lesser peak at 398.82 eV (6.66%) resembles to pyridinic nitrogen, both variations possessing lone electron pairs that can interact with metal ions. Following chromium adsorption, the N 1s spectrum of Cr@TACGC displays a notable shift; the main peak transitions to 401.81 eV (91.39%), which suggests the development of protonated or quaternary nitrogen species, attributed to electron donation to Cr^{3+} ions.[38] Furthermore, a new peak at 402.14 eV (8.61%) signals the formation of a metal–nitrogen complex, confirming the chemical interaction between the nitrogen functional groups and chromium. These changes in binding energy and composition underscore the active participation of nitrogen sites in coordinating chromium, emphasizing their significance alongside oxygen functionalities in the adsorption process. In summary, the N 1s XPS analysis reinforces the idea that nitrogen-containing groups in TACGC are vital for binding

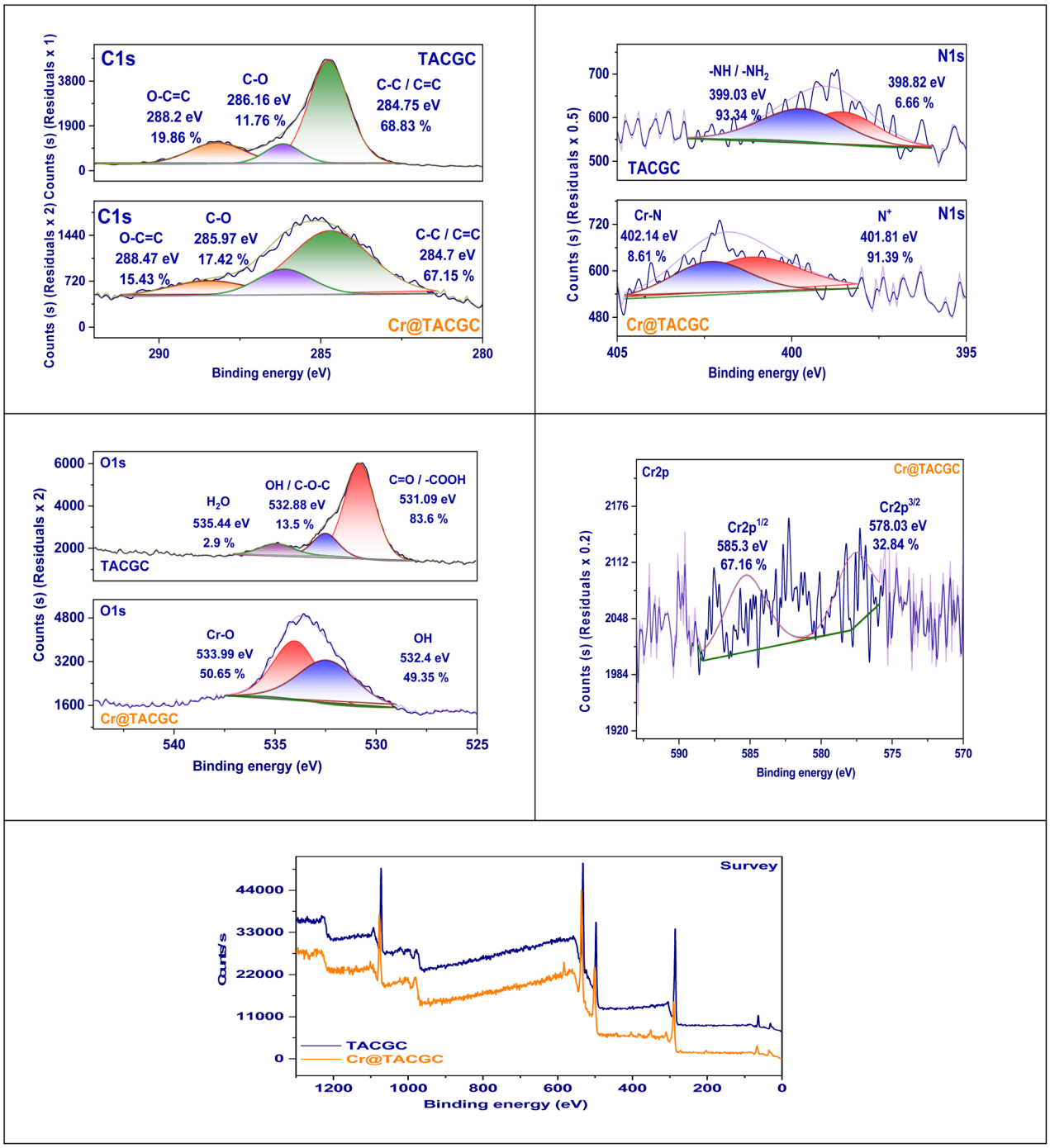

Fig. 5 XPS analysis of TACGC and Cr@TACGC.

metal ions, greatly enhancing the material's effectiveness as a biosorbent for environmental clean-up efforts.

The XPS O 1s spectra for TACGC and Cr@TACGC offer essential insights into the oxygen-containing functional groups present and their roles in chromium adsorption. The TACGC sample exhibits a significant peak at 531.09 eV, taking responsibility for 83.6% of the spectral intensity. This peak is revealing of the occurrence of carbonyl or carboxyl functional groups (C=O or –COOH). These practical groups are critical as they represent key active places for the interaction and binding of metal ions. Additionally, the peak at 532.88 eV (13.5%) corresponds to hydroxyl or ether groups (–OH or C–O–C), while a smaller peak at 535.44 eV (2.9%) likely represents adsorbed water or weakly bonded oxygen species.[39] Following chromium adsorption, the O 1s spectrum of Cr@TACGC reveals a significant alteration in the oxygen chemistry, displaying two chief peaks at 532.4 eV (49.35%) and 533.99 eV (50.65%). The observed peaks suggest the establishment of metal–oxygen (Cr–

O) bonds alongside coordinated oxygen species. This observation indicates a chemical contact among chromium ions and the oxygen practical groups present on the surface, specifically the carboxyl and hydroxyl groups. These groups appear to participate in electron donation and coordination processes with Cr^{3+} ions. The identified changes in binding energies and their redistribution demonstrate the serious role of oxygen-containing practical groups in the adsorption of chromium. This analysis underscores the effectiveness of Cr@TACGC as a bio-sorbent for the extraction of metals.

The XPS analysis of the Cr 2p region for the Cr@TACGC composite demonstrates that chromium has been successfully adsorbed onto its surface, while also shedding light on its oxidation states. The spectrum exhibits two significant peaks located at binding energies of 585.3 eV and 578.03 eV, which are associated with the Cr $2p_{1/2}$ and Cr $2p_{3/2}$ electronic states, respectively. Notably, the Cr $2p_{3/2}$ peak at 578.03 eV constitutes 32.84% of the overall signal and is indicative of trivalent chromium ions (Cr(III)). Conversely, the higher-energy peak at 585.3 eV represents 67.16% of the total signal, reinforcing the predominance of the Cr(III) oxidation state within the composite. The validation and corresponding ratios of these peaks indicate that chromium has been successfully immobilized on the TACGC surface. This process is likely facilitated by interactions that involve complexation with practical groups comprising oxygen and nitrogen atoms. The described binding mechanism facilitates the creation of a stable Cr(III) complex by the surface of the adsorbent. This observation highlights the material's capability to serve as an effective and dependable biosorbent for the removal of detrimental metals from aquatic environments.[40]

The XPS evaluation of TACGC and Cr@TACGC yields important data concerning the surface elemental composition prior to and subsequent the chromium adsorption process, suggesting that chromium has been effectively incorporated into the composite material. In the spectrum corresponding to TACGC (depicted in blue), notable peaks associated with C 1s, O 1s, and N 1s underscore the existence of carbon, oxygen, as well as nitrogen elements. The components arise from the activated carbon core combined with the biopolymer encapsulants of gum guar and carboxymethylcellulose. These materials play a crucial role in preserving structural stability and offering functional groups that are important for the process of adsorption.[41] Following the adsorption of chromium, the Cr@TACGC spectrum (shown in orange) presents new peaks in the 575–590 eV range, linked to Cr 2p, thereby confirming chromium's presence on the material's surface. Furthermore, minor changes in the relative intensities of the C, N, and O peaks indicate potential surface interactions and coordination between Cr ions and the practical groups, notably those containing oxygen as well as nitrogen. The detection of chromium-specific signals along with the variations in peak intensities emphasize the material's capability to effectively bind chromium, establishing Cr@TACGC as a chemically reactive and multifunctional biosorbent suitable for the environmental removal of metals, as illustrated in Fig. 5.

3.1.7. Zero point of charge. The zero point of charge (pH_{zpc}) for the TACGC was determined through an analysis of the relationship between ΔpH and initial pH, as illustrated in the figure provided. The pH_{zpc} is ascertained at the point where ΔpH reaches zero, which is found to be 3.59 (Fig. 6(a)). Beneath a specific pH threshold, the surface of TACGC demonstrates a net positive charge. Conversely, once the pH surpasses this threshold, the surface charge shifts to a negative state. This charge performance is particularly relevant to the adsorption processes involving chromium species. The prevalence of these species is contingent upon the pH level of the environment.[42]

3.2. Batch experiments

3.2.1. Outcome of pH. Fig. 6(b) illustrates a bar chart that analyzes the result of initial pH levels on the adsorption capability (q_e) of the TACGC in the extraction of Cr(VI). The experimental conditions spanned a pH range from 2 to 8, and the corresponding q_e values, expressed in mg g^{-1}, were systematically recorded. The results underscore the significant impact of pH on adsorption performance, revealing that maximum adsorption capacity is achieved at pH 4, where it reaches a value of 360 mg g^{-1}. This finding designates pH 4 as the optimal state for the elimination of Cr(VI) utilizing the TACGC composite.[43] At pH levels of 2 and 3, there is a noteworthy reduction in the adsorption capacity, with recorded values of 208 and 290 mg g^{-1}, individually. This indicates that lower pH conditions adversely affect the adsorption capacity. This reduction is likely attributable to excessive protonation of active sites that may compete with Cr(VI) anions for available adsorption positions. An rise in pH from 4 to 8 correlates with a significant reduction in adsorption capacity, decreasing from 360 mg g^{-1} by pH 4 to 220 mg g^{-1} at pH 8. This decline may be attributed to heightened electrostatic repulsion occurring among the negatively charged superficial of the adsorbent, which surpasses the pH_{zpc} of 3.59, and the anionic species of Cr(VI). The composite exhibits a notable degree of adsorption efficiency even at higher pH levels, indicating that alternative mechanisms, including the chemical reduction of Cr(VI) to Cr(III), complexation, and physical entrapment, could contribute to the overall removal efficacy. These results underscore that pH 4 is the most advantageous condition for maximizing Cr(VI) uptake by the TACGC.

3.2.2. Outcome of dose. The result of adsorbent dosage on the efficacy of Cr(VI) removal utilizing the TACGC composite sponge is illustrated in the figure provided. This figure presents a graphical representation of adsorption capacity (q_e, measured in mg g^{-1}) and removal efficiency (expressed as a percentage) in relation to the original concentration of the adsorbent (in mg L^{-1}). A rise in adsorbent concentration from 0.01 to 0.5 mg mL^{-1} corresponds with a significant reduction in adsorption capacity, which decreases from more than 300 mg g^{-1} to below 50 mg g^{-1}. The observed decrease can be clarified by the clustering of adsorbent units at elevated concentrations. This phenomenon reduces the effective surface area and causes the active sites to overlap, ultimately resulting in a less efficient utilization of the adsorbent. Conversely, removal efficiency

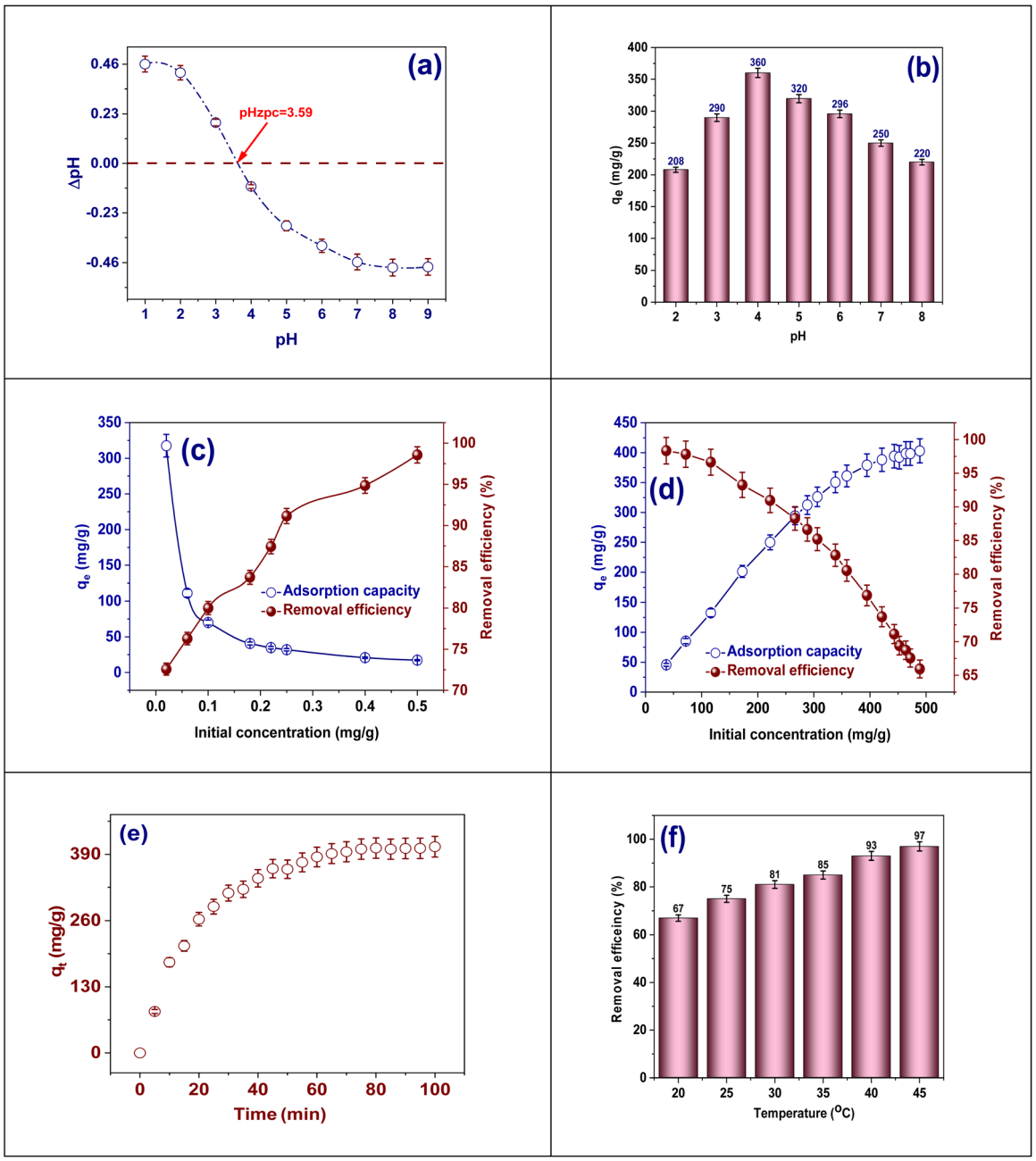

Fig. 6 (a) Resolve of pH_{ZPC} for TACGC, (b) Outcome of pH, (c) Outcome of adsorbent amount, (d) outcome of original concentration, (e) outcome of contact time, (f) outcome of temperature on Cr(VI) adsorption onto TACGC.

shows a consistent upward trend, increasing from about 75% to more than 98%, as a result of enhanced availability of binding sites that support more complete elimination of Cr(VI) from the solution.[43] These observations illustrate the common trade-off in adsorption processes between optimizing removal efficiency and preserving high adsorption capacity per unit mass. Consequently, it is essential to optimize the adsorbent dose based on whether the goal is to enhance material efficiency or achieve thorough contaminant removal (Fig. 6(c)).

3.2.3. Outcome of original concentration. Fig. 6(d) illustrates the result of the original concentration of Cr(VI) on its removal efficiency utilizing the TACGC. The analysis presents the adsorption capability (q_e, quantified in mg g^{-1}) and removal efficacy (expressed as a percentage) as they relate to diverse original concentrations of Cr(VI) (measured in mg L^{-1}).[44] An analysis of the data reveals that as the original concentration of Cr(VI) escalates from 25 to 500 mg L^{-1}, the adsorption capability demonstrates a consistent increase, ultimately reaching a maximum of approximately 430 mg g^{-1} at the highest concentration. This observed trend can be attributed to an enhanced driving force for mass transfer along with a greater obtainability of Cr(VI) ions, which collectively promote their diffusion towards the active places of the adsorbent. Conversely, although the removal efficacy starts above 95% at lower

concentrations, it progressively decreases with an increase in concentration, dropping to below 70% at the maximum concentration confirmed. The observed decrease can be credited to the insufficient obtainability of adsorption places, which cannot effectively hold the excess Cr(VI) ions when present in higher concentrations, leading to a saturation of the surface. These findings suggest that while higher initial concentrations can boost the adsorption capacity of TACGC, the overall removal efficiency decreases due to a limitation in available sites. This underscores the necessity of optimizing concentration levels to achieve the best performance in real-world applications.

3.2.4. Outcome of contact time. Fig. 6(e) offerings an examination of the influence of contact duration on the adsorption process of Cr(VI) onto the TACGC composite sponge, highlighting the adsorption capability (q_t, expressed in mg g^{-1}) over a time frame measured in minutes. The results indicate a prompt escalation in the absorption of Cr(VI) during the initial stages, notably within the first 30 min, where the adsorption capability involvements a important increase. This phenomenon can be accredited to the high obtainability of active places present on the surface of the TACGC sponge during this period. As time continues, the rate of adsorption gradually decreases, and the curve starts to plateau, representing that the active places are nearing saturation and equilibrium is being achieved. After 80 min, the adsorption capacity stabilizes at approximately 390 mg g^{-1}, suggesting that equilibrium has been reached, resulting in no significant further uptake. This pattern corresponds with typical pseudo-second-order kinetic behavior, emphasizing the role of chemisorption.[45] The initial fast adsorption followed by a gradual leveling off illustrates the effectiveness of TACGC in swiftly removing Cr(VI) from the solution and confirms that a contact time of around 80–90 min is adequate for attaining optimal removal efficacy under the specified conditions.

3.2.5. Outcome of temperature. Fig. 6(f) exemplifies a bar graph demonstrating the impact of temperature on the elimination efficiency of Cr(VI) when utilizing the TACGC composite sponge, inside a temperature from 20 to 45 °C. The results reveal a different positive correlation between temperature and elimination efficacy, implying that the adsorption mechanism operates under endothermic conditions. At 20 °C, the removal efficiency stands at 67%, but this figure increases progressively with rising temperatures reaching 75% at 25 °C, 81% at 30 °C, 85% at 35 °C, and peaking at 97% at 45 °C. The enhanced elimination of Cr(VI) at increased temperatures can be elucidated through various mechanisms. Elevated temperatures elevate the mobility and diffusion rates of Cr(VI) ions, facilitating their movement toward the surface of the adsorbent. This thermal increase also promotes greater accessibility to active sites by expanding or loosening the structure of the composite. Furthermore, it may lead to intensified interactions, including chemisorption or surface complexation.[46] These results imply that elevated temperatures improve the adsorption process, supporting the notion that TACGC functions effectively as a heat-assisted system, and suggesting that its operational performance can be optimized under moderate thermal conditions.

3.3. Adsorption isotherm

The request of adsorption isotherm models is vital for sympathetic the equilibrium dynamics and the mechanisms of surface communications that dictate the adsorption behavior of Cr(VI) onto the TACGC. These models deliver invaluable information regarding adsorption capacity, surface properties, and the nature of the binding process, which facilitates the effective design and optimization of treatment systems. The Langmuir isotherm model proposes that adsorption receipts in a monolayer format on a homogenous surface that has a limited number of active sites. This framework assists in determining both the maximum capacity for adsorption and the binding affinity of TACGC concerning Cr(VI).[47] In contrast, the model of Freundlich isotherm characterizes multilayer adsorption occurring on a varied surface, signifying variations in the energy of adsorption sites and their affinity to adsorbates. The constants associated with this model reflect both the strength and the favorability of the adsorption mechanism.[48] The Dubinin–Radushkevich (D–R) model is utilized to distinguish between physical and chemical adsorption through the evaluation of the mean free energy (E). By calculating the mean free energy (E), the Dubinin–Radushkevich (D–R) model is used to differentiate between chemical and physical adsorption. Specifically, values that are below 8 kJ mol^{-1} indicate a predominance of physisorption, whereas values exceeding this threshold are indicative of chemisorption.[49] The Temkin isotherm provides a framework for understanding the interactions present among the adsorbate and adsorbent, suggesting that the heat released throughout the adsorption procedure decreases in a linear way as the attention increases. This relationship offers valuable visions into the energy distribution and the relative intensity of the connections involved.[50] Furthermore, the Jossens isotherm, based on energy distribution theory, offers a deeper sympathetic of heterogeneous surfaces and cooperative adsorption effects, implying that the TACGC sponge exhibits a complex and energetically varied adsorption profile.[51] Together, these models create a comprehensive framework for characterizing and enhancing Cr(VI) adsorption performance, enabling the assessment of adsorption mechanisms, surface behavior, and system design across diverse environmental conditions (Table S4).

There are numerous important benefits to employing the Langmuir adsorption isotherm model when removing Cr(VI) with the TACGC. This model provides a clear theoretical foundation for efficiently evaluating the adsorption features since it assumes that monolayer adsorption occurs on a small number of uniform surface locations.[47] The findings reveal that the experimentally determined maximum adsorption capacity (q_m exp) is 402.97 mg g^{-1}, closely identical the theoretical q_m value of 404.87 mg g^{-1}. This near equivalence illustrates a significant consistency between the empirical data and the model's projections, as detailed in Table S5. The Langmuir constant (K_L) of 0.05896 L mg^{-1} indicates a moderate empathy between Cr(VI) and the active sites on TACGC, suggesting a significant interaction that does not result in irreversible binding. Additionally, the dimensionless separation factor (R_L) with a value of 0.077,

falling among 0 and 1, signifies that the adsorption procedure is promising under the specified experimental conditions. In summary, the Langmuir model not only provides a precise measurement of adsorption capacity but also enhances the understanding of surface homogeneity, site saturation, and binding efficiency, thus serving as an effective instrument for optimizing system design and forecasting performance in practical applications aimed at Cr(VI) remediation using TACGC, as thorough in Table S6.

Applying the Freundlich adsorption isotherm model to investigate the efficacy of the TACGC in removing Cr(VI) offers significant advantages for elucidating the surface belongings of the solid and the mechanisms driving its adsorption processes. In contrast to the model of Langmuir, which assumes a uniform surface with adsorption occurring in a single layer, the model of Freundlich is based on experiential data and is applicable to heterogeneous surfaces that feature varying energy sites. This characteristic enables the Freundlich model to account for multilayer adsorption processes. The Freundlich constant, with a value of $n = 3.32$, designates that the adsorption procedure is both favorable and significant. This is evidenced by the fact that values exceeding one reflect pronounced interactions among the adsorbate and the adsorbent.[48] The Freundlich constant, represented as $K_F = 91.65$ (mg g^{-1}) (L mg^{-1})$^{1/n}$, quantitatively reflects the adsorption capability of the sponge, demonstrating its significant affinity for Cr(VI) ions. Utilizing the Freundlich model elucidates the existence of various binding sites on the TACGC and reinforces the idea that Cr(VI) removal happens not only through surface adsorption but also potentially through complex interactions involving multiple layers or energy levels. This characteristic of the model proves to be particularly advantageous for simulating authentic environmental conditions characterized by surface heterogeneity, as demonstrated in Fig. 7(a).

The request of the Dubinin–Radushkevich (D–R) isotherm model for investigating the adsorption of Cr(VI) on the TACGC provides a comprehensive insight into the fundamental mechanisms and energy dynamics involved in the adsorption process. This analysis goes deeper than just considering the surface topology, highlighting the complexities of the interactions at play.[49] In contrast to the models of Langmuir as well as Freundlich, which assume of a homogeneous surface and consistent adsorption potential, the D–R model excels in distinguishing among physical as well as chemical adsorption procedures. The data reveals a maximum adsorption capability (Q_{DR}) of 377.84 mg g^{-1}, underscoring the noteworthy uptake efficiency of TACGC. Furthermore, the mean free energy of adsorption (E_a), intended from the model, is determined to be 33.6 kJ mol^{-1}. This figure is significantly higher than the conventional value of 8 kJ mol^{-1}, indicating that the adsorption of Cr(VI) is predominantly driven by chemisorption. This procedure likely involves strong connections, which may

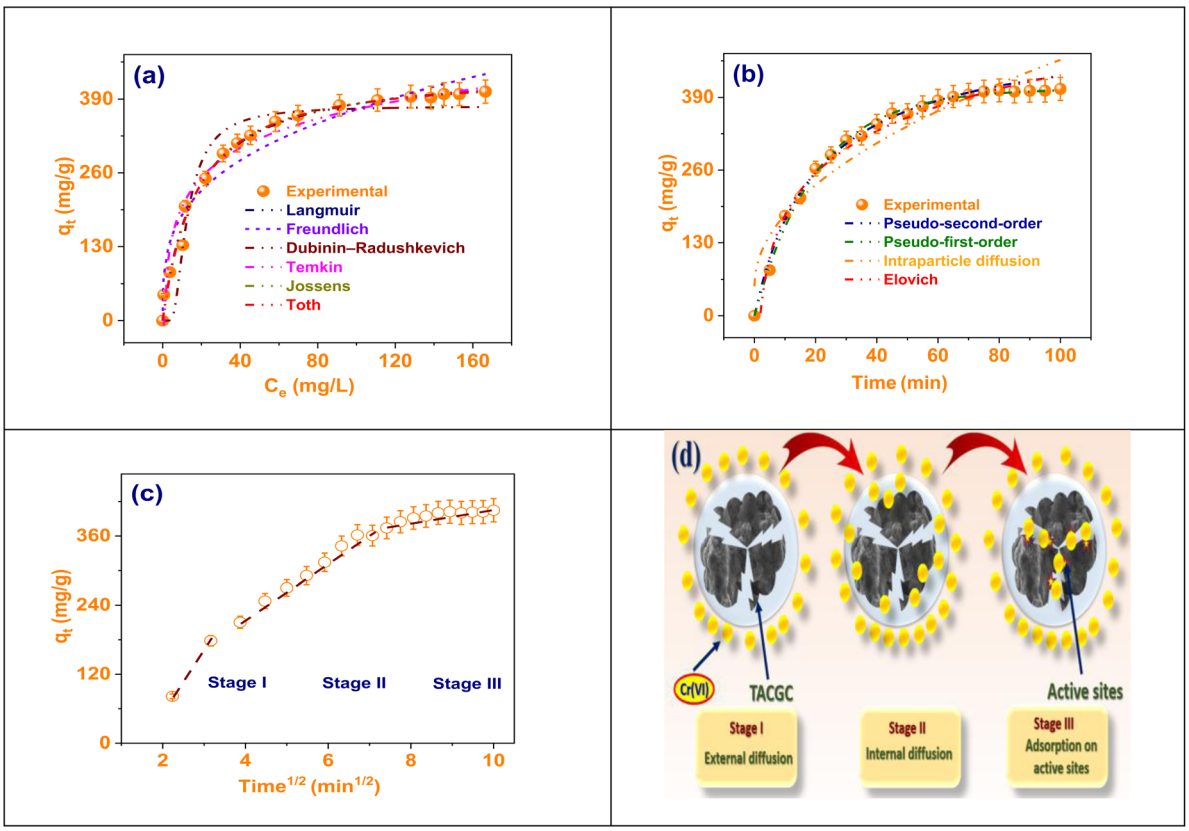

Fig. 7 (a) Adsorption isotherms models, (b) adsorption kinetics models, (c) intraparticle diffusion, and (d) diagram of intraparticle diffusion on adsorption of Cr(VI) onto TACGC.

comprise mechanisms such as ion exchange, complexation, or electron sharing. The identified energy level designates that the adsorption device is not merely reliant on weak van der Waals interactions; rather, it engages stronger and more defined chemical bonds.

The application of the Temkin adsorption isotherm model for the extraction of Cr(VI) using the TACGC offers multiple advantages, as it accounts for the interactions between the adsorbates and the adsorbents, in addition to variations in adsorption energy in relation to surface coverage. These factors are often neglected by other models, such as the Langmuir isotherm.[50] The model of Temkin posits that as the surface approaches saturation, the heat of adsorption decreases linearly, which better represents adsorption dynamics on heterogeneous surfaces. In the data presented, the Temkin binding energy constant (b_T) is recorded at 33.22 J mol^{-1}, signifying a moderate strength of communication among Cr(VI) and the TACGC surface. The equilibrium binding constant (K_t) value of 1.46 L mol^{-1} suggests a significant level of affinity between the adsorbent and Cr(VI) ions. This strong binding characteristic indicates effective interactions, which may improve the adsorption procedure within the given system. The results indicate that the adsorption procedure is administrated by both physical mechanisms and chemical interactions, which are determined by the variation in surface energy distribution. The model of Temkin delivers important visions into the thermodynamic properties associated with the adsorption of Cr(VI). It highlights the variation in interaction energies across the adsorption procedure, which is instrumental in enhancing the design of optimized adsorption systems that incorporate TACGC materials.

The utilization of the Jossens adsorption isotherm model in the context of Cr(VI) adsorption *via* the TACGC offers significant analytical perspectives regarding the heterogeneity of the surface and the distribution of energy across the adsorption sites. In contrast to traditional isotherm models that presume uniform energy across sites, the Jossens model is rooted in energy distribution theory, making it particularly effective for examining systems with complex surface characteristics. The Jossens equilibrium constant (K = 24.49 L mg^{-1}) signifies a significant interaction between Cr(VI) ions and the active sites present on the TACGC sponge. Additionally, the very low n value (0.047) highlights a restricted energy distribution, suggesting that adsorption primarily involves high-energy binding sites. This limited distribution could indicate specific or selective binding interactions, possibly involving chemisorption or strong electrostatic forces.[51] The Jossens model illustrates not only the presence of advantageous energetic interactions but also confirms the heterogeneous surface architecture of the TACGC sponge (Fig. 7(a)).

The Toth adsorption isotherm model presents notable advantages in the examination of the adsorption process of Cr(VI) onto the TACGC composite sponge, particularly in its ability to represent systems that do not conform to ideal monolayer adsorption due to varying surface characteristics. This model serves as a generalized approach that effectively connects the Langmuir and Freundlich isotherms, making it particularly relevant when the adsorption surface comprises places with varied energy stages. The information reveals that the sponge exhibits a maximum adsorption capability (q_m) of 438.94 mg g^{-1}, importance its significant efficacy in the uptake of Cr(VI). Additionally, the Toth constant (K_t = 21.54 L mg^{-1}) suggests a pronounced affinity between the Cr(VI) ions and the TACGC surface. Additionally, the Toth exponent (t = 1.06), which is close to 1, implies that the system behaves similarly to Langmuir-type adsorption while exhibiting minor heterogeneity among the active sites. This balance enhances the Toth model's capacity to accurately describe real-world systems, which typically lack perfect surface uniformity. Therefore, the utilization of the Toth isotherm model facilitates a more precise and flexible assessment of Cr(VI) adsorption efficiency on TACGC, which further bolsters its applicability in intricate environmental remediation initiatives.[51]

The evaluation of adsorption isotherms reveals that the TACGC composite sponge exhibits significantly enhanced performance in the adsorption of Cr(VI) compared to the unmodified TAC. This superior efficacy is attributed to the synergistic interactions between the activated carbon core and the functionalized GG–CMC–IA polymer matrix. According to the Langmuir model, TACGC demonstrates a notable increase in monolayer adsorption capacity, with values of q_m = 404.87 mg g^{-1} for TACGC, in contrast to 322.7 mg g^{-1} for TAC Fig. S1(a). Additionally, TACGC shows an increased affinity constant (K_L = 0.05896 L mg^{-1} *versus* 0.029 L mg^{-1}) and a substantially lower R_L value (0.077 as opposed to 0.62), suggesting a more favorable and robust binding process. The advantages of TACGC are further substantiated by the Freundlich parameters, which indicate a higher heterogeneity factor (n = 3.32) and nearly double the adsorption capacity at low concentrations (K_F = 91.65 mg g^{-1} (L mg^{-1})$^{1/n}$ compared to 53.19 mg g^{-1} (L mg^{-1})$^{1/n}$).[51] The Dubinin–Radushkevich isotherm analysis corroborates the pronounced chemisorptive characteristics of TACGC, which reveals greater sorption energy (E_a = 33.6 kJ mol^{-1} as opposed to 31.4 kJ mol^{-1}) and an elevated maximum capacity (Q_{DR} = 377.84 mg g^{-1} contrasted with 312.6 mg g^{-1}). Furthermore, both the Temkin and Jossens models signify stronger adsorbate–adsorbent interactions for the composite sponge, evidenced by a higher K_T (1.46 relative to 0.244 L mol^{-1}), an increased b_T (33.22 *versus* 27.58 J mol^{-1}), and a significantly elevated Jossens equilibrium constant (24.49 compared to 7.91 L mg^{-1}). The Toth model reinforces these findings, indicating the superior structural homogeneity and enhanced affinity of TACGC, which is characterized by a higher maximum capacity (438.94 mg g^{-1} as opposed to 322.16 mg g^{-1}), a stronger binding constant (K_T = 21.54 relative to 15.85 L mg^{-1}), and a t value approaching unity (1.06), suggesting a more uniform distribution of active sites post-polymer encapsulation. Collectively, these parameters affirm that the TACGC composite sponge offers improved pore accessibility, enhanced surface functionality, stronger electrostatic and complexation interactions, as well as more energetically favorable adsorption sites in comparison to TAC alone, culminating in significantly elevated efficiency for Cr(VI) removal (Table S6).

3.4. Adsorption kinetics

The utilization models of adsorption kinetics, including pseudo-first-order,[52] pseudo-second-order,[53] Intraparticle diffusion,[54] and Elovich, is essential for elucidating the rate, mechanisms, and controlling factors involved in the adsorption of Cr(VI) onto the TACGC.[55] The pseudo-first-order model is based on the concept that the rate of adsorption is directly proportional to the quantity of vacant places obtainable for occupation, which is often associated with physisorption mechanisms. An inadequate fit to this model could suggest that physical interactions by themselves may not sufficiently explain the uptake of Cr(VI). In contrast, the model of pseudo-second-order proposes that the adsorption mechanism is primarily driven by chemisorption, characterized by the exchange or distribution of electrons among Cr(VI) ions and the functional groups situated on the surface of TACGC. A strong correlation with this model suggests that chemical interactions are pivotal in determining the adsorption rate. The Intraparticle diffusion model assesses the role of Cr(VI) ion diffusion into the internal pores of the sponge as a potential limiting factor in the overall reaction rate. A multi-linear plot would suggest that the adsorption procedure happens in multiple stages, encompassing both external film diffusion and intraparticle transport dynamics. Additionally, the model of Elovich shows to be exceptionally insightful for elucidating the process of adsorption happening on heterogeneous surfaces considered by varying adsorption energy. This model is regularly applicable to chemisorption phenomena on materials exhibiting considerable surface irregularities. A solid fit with the Elovich equation indicates that factors such as surface activation and varying interaction energies are crucial in the adsorption of Cr(VI). These models serve a dual purpose: they enable precise measurement of adsorption kinetics and assist in determining the mechanisms governing the adsorption process. Specifically, they can indicate if the process is predominantly influenced by diffusion, characterized by chemical interactions, or affected by the variability in surface characteristics. This insight is crucial for advancing our comprehension and optimizing the effectiveness of the TACGC sponge in the removal of Cr(VI) (Table S4).

The application of the pseudo-first-order kinetic model in examining the adsorption of Cr(VI) onto the TACGC yields valued visions into the preliminary rate and underlying mechanism of the adsorption process.[52] This model is founded on the hypothesis that the variation in the adsorption rate over time is directly related to the quantity of available active sites. This relationship generally corresponds with physisorption mechanisms, considered by relatively weak van der Waals forces (Table S5). The data indicate a rate constant (K_1) of 0.0495×10^{-2} min^{-1}, suggesting a relatively slow physisorption rate under the analyzed conditions. Although the pseudo-first-order model may not completely encapsulate the entire adsorption phenomenon, particularly in instances where chemisorption plays a major role, it is particularly effective in delineating the initial phases of adsorption, wherein physical interactions and surface diffusion are expected to dominate. Furthermore, comparing this model with other kinetic frameworks allows researchers to assess whether physical or chemical interactions primarily influence the overall process. As a result, employing the pseudo-first-order model facilitates a deeper mechanistic comprehension of Cr(VI) adsorption on TACGC, especially in scenarios where the dynamics of initial surface interactions are of significant importance (Table S7).

The kinetic model of pseudo-second-order is utilized to elucidate the way of Cr(VI) adsorption on the TACGC, offering insights into the chemisorption mechanism. In this context, the adsorption rate is determined by the chemical bonds formed through electron sharing or exchange between Cr(VI) ions and the active practical groups present on the TACGC surface.[53] This model posits that the capacity for adsorption is directly related to the square of the number of unoccupied sites, making it particularly applicable in scenarios dominated by chemical interactions. Analysis of the provided data reveals a rate constant (K_2) of 9.68136×10^{-5} g mg^{-1} min^{-1} as well as an equilibrium adsorption capability (q_e) of 404.85 mg g^{-1}, which is consistent with empirical measurements. This close correlation validates that the adsorption dynamics obey to second-order kinetics, highlighting the significance of chemical reactions occurring at the adsorbent surface. The primary advantage of this model is its capacity to accurately forecast adsorption behavior over time, facilitate the design of optimal contact durations, and elucidate surface interaction characteristics. This makes it particularly advantageous for enhancing the efficacy of TACGC in the elimination of Cr(VI) from water solutions, as proved in Fig. 7(b).

The investigation of Cr(VI) adsorption onto the TACGC composite sponge using the intraparticle diffusion kinetic model offers crucial information on the fundamental diffusion pathways that control the adsorption procedure. This model plays a crucial role in identifying whether the movement of Cr(VI) ions within the adsorbent's internal structure, rather than adsorption on its outside surface, is the rate-limiting step. The data indicates that the intraparticle diffusion rate constant (K_i) has a recorded value of 40.38 mg g^{-1} $min^{-1/2}$. Additionally, the width of the border layer (X) is measured at 57.78 mg g^{-1}.[54] This notable value proposes a resistance to external mass transfer and underscores the substantial influence of boundary layer diffusion. The model indicates that if intraparticle diffusion is the only factor governing the rate of the process, the plotted graph of the amount adsorbed against time squared would commence from the origin. However, a non-zero intercept indicates that multiple stages are at play, including initial surface adsorption followed by deeper intraparticle diffusion. Employing this model facilitates a distinct delineation between the impacts of external and internal diffusion, aids in the optimization of variables such as particle size and agitation speed, and improves the comprehension of the adsorption mechanism. This is especially pertinent for advancing TACGC-based systems designed to efficiently eliminate Cr(VI) from water sources.

Employing the model of Elovich kinetic to examine the adsorption of Cr(VI) onto the TACGC composite sponge offers significant advantages for understanding adsorption dynamics on surfaces characterized by energetic heterogeneity. This

method is mainly advantageous in contexts where chemisorption plays a dominant role in the adsorption procedure. This model operates under the hypothesis that the adsorption rate decreases exponentially over time, a phenomenon attributed to the gradual saturation of high-energy sites. This behavior is typical of adsorbents exhibiting diverse active sites, such as TACGC. According to the data provided, the original adsorption rate (α) is resolute to be 0.0048 mg g^{-1} min^{-1}, while the desorption constant (β) is recorded at 108.58 g mg^{-1}. These figures suggest a relatively slow, yet energetically favorable adsorption process that becomes progressively slower as the surface becomes more populated (Table S7). The Elovich model demonstrates to be notably useful in scenarios where the adsorption process deviates from simple first- or second-order kinetics. Additionally, it is effective in cases where the adsorption rate is influenced by variations in surface activation and energy distribution. The robustness of this study is attributed to its ability to clarify the complex kinetics that govern the adsorption process of Cr(VI) onto TACGC as a role of time. This investigation offers significant insights into activation energies, the variability of surface characteristics, and the nature of connections that occur among the adsorbate and the adsorbent. The Elovich model aids as an important tool for studying and improving adsorption mechanisms within the context of real-world water treatment applications.[55]

The kinetic parameters provide compelling evidence that the TACGC composite sponge exhibits markedly superior adsorption efficiency for Cr(VI) when compared to raw TAC. This enhancement can be attributed to the composite's synergistic structural and chemical properties. Notably, the pseudo-second-order model, which is representative of systems governed by chemisorption, reveals a significantly higher rate constant for TACGC ($K_2 = 9.68136 \times 10^{-2}$ g mg^{-1} min^{-1}) in contrast to that of TAC (5.68×10^{-5} g mg^{-1} min^{-1}). This finding substantiates the notion that TACGC engages in considerably more rapid electron-sharing or electron–exchange interactions with chromium species (Fig. S1(b)). Additionally, TACGC demonstrates a greater theoretical equilibrium uptake (q_e = 404.85 mg g^{-1}) relative to TAC (323.2 mg g^{-1}), implying a higher density of active sites and improved utilization of surface functionalities. Further supporting this advantage is the intra-particle diffusion model, which indicates that TACGC possesses a higher diffusion rate constant (K_i = 40.38 mg g^{-1} $min^{-1/2}$) compared to TAC (35.44 mg g^{-1} $min^{-1/2}$). This suggests that the mesoporous polymer-carbon framework of the composite promotes more efficient transport of Cr(VI) into its internal pores. The observation of an elevated boundary layer thickness (X = 57.78 mg g^{-1} for TACGC *vs.* 36.82 mg g^{-1} for TAC) also points to a more pronounced external–surface interaction zone, which aligns with enhanced electrostatic attraction and redox properties.[51] Moreover, the Elovich model, indicative of heterogeneous chemisorption, presents higher values for α (0.0048 mg g^{-1} min^{-1} for TACGC compared to 0.002 for TAC), reinforcing the conclusion that TACGC offers more energetically favorable active sites for the initial uptake of chromium. Lastly, the experimental adsorption capacity adheres to these observed trends, with TACGC achieving a capacity of 406.22 mg g^{-1} *versus* 326.6 mg g^{-1} for TAC, thereby indicating a considerable enhancement in both the rate of adsorption and maximum capacity. In aggregate, these kinetic parameters demonstrate that the GG–CMC–IA polymer encapsulation not only preserves but significantly augments the accessibility, reactivity, and diffusivity of the activated carbon, thereby establishing TACGC as a markedly more effective material for the removal of Cr(VI) than TAC alone (Table S7).

3.5. Mechanism of diffusion

Regarding the adsorption of Cr(VI) onto the TACGC, the plot of intraparticle diffusion is depicted in the figure.[54] The graph presents an analysis of the association among adsorption capacity (q_t) and the square root of time ($t^{1/2}$), a commonly employed method for evaluating the diffusion mechanism and identifying possible rate-limiting factors in the adsorption procedure. The curve clearly segments into three distinct linear phases: Stage I, Stage II, and Stage III, with each segment representing a specific stage in the broader adsorption mechanism. Stage I indicates the initial phase characterized by a rapid uptake of Cr(VI) ions, attributed to boundary layer or external surface diffusion. During this stage, Cr(VI) ions are quickly absorbed onto the TACGC's outer surface, taking advantage of the readily available active sites, resulting in a steep slope on the graph. Stage II reflects the intraparticle diffusion phase, where Cr(VI) ions begin to penetrate the sponge's internal pores. This phase occurs at a slower rate and typically controls the overall adsorption kinetics (Fig. S1(c)). Finally, Stage III represents the equilibrium phase, where the rate of diffusion decreases, and the adsorption capacity stabilizes as most active sites become saturated. The significant finding that the lines fail to meet at the origin proposes that intraparticle diffusion is not solely responsible for the rate-limiting factors involved. Both boundary layer resistance and surface adsorption are also significant contributors to the overall kinetics. This complex multi-phase process underscores the intricacies related with the Cr(VI) adsorption on the TACGC. It underscores the critical need for optimizing various operational parameters, including contact time, adsorbent dosage, and mixing techniques, to efficiently advance the efficacy of removal, as illustrated in Fig. 7(c and d).

3.6. Adsorption thermodynamics

The figure presented illustrates the relationship between temperature and the adsorption of Cr(VI) onto the TACGC, analyzed through Van't Hoff, Arrhenius, and Gibbs free energy methodologies. In Fig. 8(a), the Van't Hoff graph demonstrates a linear connection among $\ln K_c$ and $1/T$, facilitating the determination of a positive enthalpy change ($\Delta H°$ = 93.45 kJ mol^{-1}) along with a positive entropy change ($\Delta S°$ = 325.57 J mol^{-1} K), as detailed in Table S8. This suggests that the adsorption mechanism is endothermic in nature and correlates with a rise in disorder at the solid–liquid boundary. This phenomenon is probably linked to the desolvation of Cr(VI) ions, which subsequently leads to structural alterations within the sponge matrix. Typically, physisorption processes are

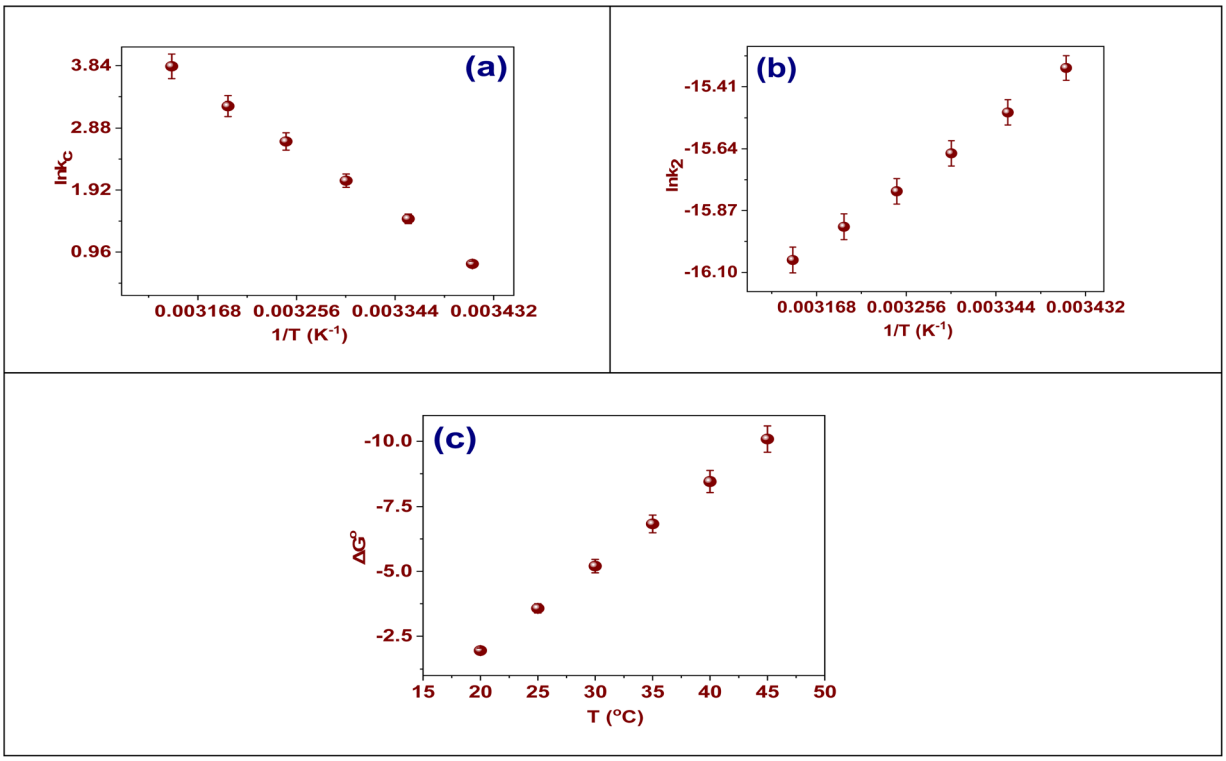

Fig. 8 (a) Van't Hoff plot, (b) Arrhenius plot, and (c) effect of temperature on $\Delta G°$.

characterized by enthalpy values below 40 kJ mol^{-1}, whereas chemisorption generally falls within the range of 40 to 200 kJ mol^{-1}, attributed to the establishment of stronger inner-sphere interactions between the adsorbate and the surface functional groups. In the present study, Cr(VI) species ($HCrO_4^-$/$Cr_2O_7^{2-}$) are subjected to a two-step mechanism: an initial electrostatic attraction to the protonated TACGC surface, followed by an *in situ* reduction to Cr(III) facilitated by electron-rich oxygenated and nitrogen-containing functional groups, culminating in subsequent chelation or inner-sphere complexation with carboxyl and hydroxyl groups within the GG–CMC–IA matrix. This redox–complexation pathway necessitates considerable energy input, as evidenced by the elevated $\Delta H°$ value. Moreover, the significant positive entropy change ($\Delta S° = +325.7$ J mol^{-1} K^{-1}) further corroborates this hypothesis; the reduction of Cr(VI) to Cr(III) results in the release of bound water molecules and an increase in disorder at the solid–solution interface. The literature corroborates the presence of comparably high enthalpy values (70–120 kJ mol^{-1}) associated with Cr(VI) adsorption systems characterized by redox transformations and robust coordination interactions. Consequently, the reported $\Delta H°$ is consistent with the anticipated thermodynamic profile of Cr(VI) chemisorption involving reduction, surface complexation, and strong ligand binding on functionalized carbon–polymer composites.

In Fig. 8(b), the Arrhenius plot illustrating $\ln k_2$ *vs.* $1/T$ demonstrates a clear linear correlation. This relationship is instrumental in calculating the activation energy (E_a), which is determined to be 44.8 kJ mol^{-1}, as shown in the same figure. The significance of this activation energy lies in its exceedance of the conventional benchmark of 40 kJ mol^{-1}, a critical value that differentiates physical adsorption from chemical adsorption. Consequently, this result suggests that the mechanism governing the removal of Cr(VI) onto TACGC is predominantly driven by chemisorption.[56] Chemisorption is characterized by stronger interactions, including electron sharing, redox reactions, and surface complexation, which are consistent with the redox-active sites present in tobacco-derived activated carbon and the functional groups (–COOH and –OH) from the polymer matrix.[57] In summary, the data from the three plots collectively demonstrates that the Cr(VI) adsorption onto TACGC is characterized as an endothermic process that is both spontaneous and chemically driven. This phenomenon exhibits an increase at elevated temperatures, as depicted in Fig. 8(c).

Fig. 8(c) illustrates a noticeable trend in the Gibbs free energy change ($\Delta G°$), indicating that as the temperature rises, the values of $\Delta G°$ progressively shift toward more negative values. Specifically, these values demonstrate a range approximately from −2 to −10 kJ mol^{-1} throughout the temperature range examined.[58] This observation suggests that the adsorption process exhibits spontaneity and becomes increasingly thermodynamically favorable with rising temperatures.

3.7. Interaction mechanism

The interaction mechanism involved between Cr(VI) and TACGC composite, is influenced by various factors, including electrostatic attraction, redox transformations, surface complexation, and diffusion-driven entrapment. Under optimal, mildly acidic

conditions, specifically around a pH of 4, the surface of the composite acquires a positive charge as the pH approaches the point of zero charge of the material ($pH_{zpc} = 3.59$). This alteration in surface charge enhances the electrostatic attraction towards the predominant anionic forms of Cr(VI), specifically $HCrO_4^-$ and $Cr_2O_7^{2-}$. These anions initially approach the protonated polymer shell before migrating inward through mesoporous and microporous pathways present in the activated carbon core. Upon contact with the abundant electron-rich functional groups containing oxygen and nitrogen (such as –OH, –COOH, C=O, and amine-like entities), Cr(VI) is subjected to reduction to its trivalent form (Cr(III)), a process that is facilitated by the redox-active nature of the carbon surface. The resultant Cr(III) subsequently forms stable inner-sphere complexes with the carboxyl and hydroxyl groups located within the GG–CMC matrix, leading to significant chemisorption. Beyond these chemical interactions, the porous architecture of the TACGC, reinforced through crosslinking with itaconic acid, permits additional physical entrapment and hydrogen bonding, thereby enhancing metal uptake. While the presence of competing ions such as sodium (Na^+) can reduce the efficiency of this process by compressing the electrical double layer or competing with Cr(III) for negatively charged sites, the maintenance of optimal pH levels, facilitation of *in situ* reduction of Cr(VI), or incorporation of selective functional groups may alleviate this issue. Ultimately, the synergistic interaction of electrostatic forces, redox reactions, complexation phenomena, and diffusion processes collectively enables the effective penetration of chromium species into the encapsulated matrix, resulting in a strong binding capacity within the TACGC and culminating in a highly efficient adsorption mechanism.[59]

3.8. Effect of coexisting ions

Different concentrations of sodium chloride (NaCl) solutions, specifically between 10 and 40 g L^{-1}, were added to an ion-containing solution. This experiment was designed to evaluate how variations in ionic strength influenced the adsorption behavior of Cr(VI) ions when utilizing a TACGC. The examination presented in Fig. 9(a) indicates a pronounced reduction in the removal efficacy of Cr(VI) correlated with an increase in ionic strength. Significantly, the adsorption capacity experienced notable deterioration once the concentration of Na^+ attained 50 g L^{-1}. The results indicate that the incorporation of NaCl unfavorably affected the electrostatic connections between Cr(VI) and the TACGC. Furthermore, this observation lends credence to the notion that a chemical communication takes place among Cr(VI) ions and the TACGC.[60]

Fig. 9(b) offers a comprehensive inspection of the impact that different salts, particularly NaCl, Na_2CO_3, and KNO_3, have on the adsorption capacity of a TACGC for Cr(VI) ions. This analysis is conducted under a regulated temperature of 25 °C besides a pH of 4, allowing for a controlled assessment of the interactions involved. The different ions produced by the dissociation of these salts are responsible for the variances in the effectiveness of Cr(VI) removal, underscoring the intricate interactions at work. The efficiency of Cr(VI) ion removal exhibited a pronounced correlation with the inclusion of 0.1 M NaCl. This influence became chiefly apparent when an adsorbent dosage of 0.02 g was employed, while consistently maintaining the pH at 4, adhering to established temperature situations, and utilizing a sample capacity of 25 mL.[61] The findings suggest that sodium chloride and Cr(VI) ions interact significantly, which may have an effect on the availability of essential active binding locations needed for the adsorption mechanism. The efficacy of adsorption seems to be barely affected by the presence of 0.1 M Na_2CO_3 in the aqueous solution. However, the adsorption capacity for Cr(VI) is decreased at the addition of 0.1 M KNO_3, indicating a significant interaction involving KNO_3 as well as the adsorbent surface.

3.9. Effect on real water samples

Using the batch equilibrium approach, the efficacy of the synthesized TACGC in removing Cr(VI) from a variety of water

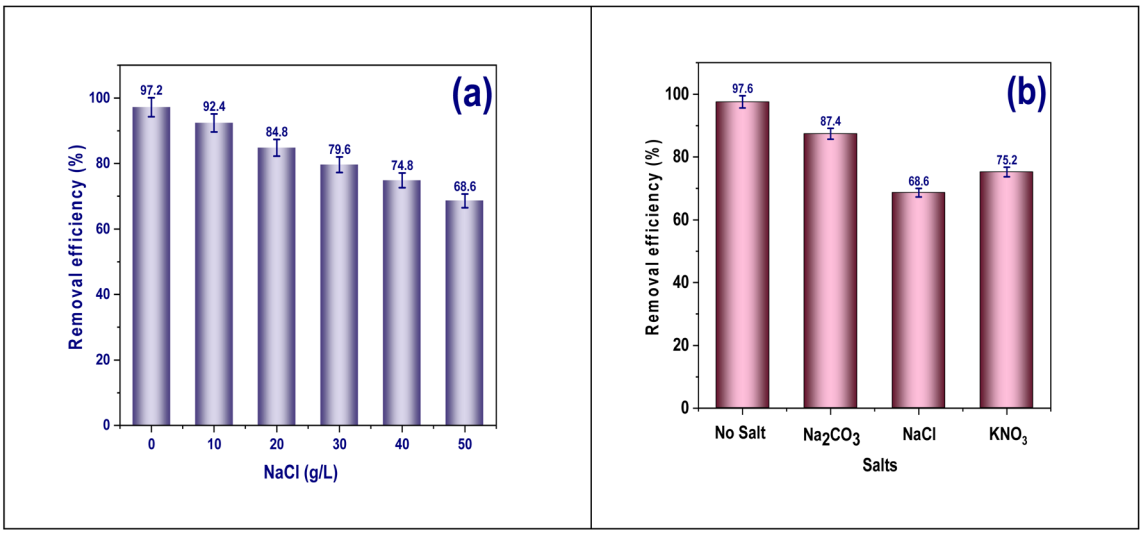

Fig. 9 (a) The influence of NaCl, (b) the influence of different salts on the adsorption of Cr(VI) ions on TACGC.

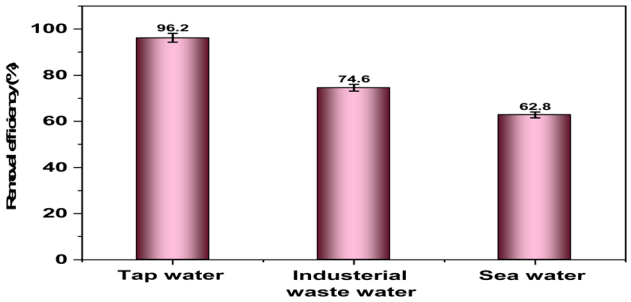

Fig. 10 Result of Cr(VI) adsorption from real water samples *via* TACGC.

sources, such as seawater, industrial effluent, and potable tap water, was methodically assessed. For the removal of Cr(VI), an exact mass of 200.0 ± 1.0 mg of the TACGC was meticulously chosen for the analysis. A 100 mL solution containing chromium in the hexavalent state (Cr(VI)) was systematically mixed with a water sample along with a predetermined quantity of sponge material. The removal process of Cr(VI) from various water sources, including tap water, seawater, and wastewater, was directed concluded a shaking period of 100 min. The removal efficiencies recorded after the completion of the third extraction cycle were as follows: 74.6% for wastewater, 96.2% for tap water, and 62.8% for seawater.[39] The findings suggest a substantial impact of water source on extraction efficiency. Interestingly, both tap water and wastewater showed higher recovery rates than seawater, highlighting a complex link between the kind of water used and the extraction process' efficacy (Fig. 10).

3.10. Reusability

In this investigation, 0.02 g of TACGC was used to treat a 50 mL aqueous solution containing 100 mg L^{-1} of Cr(VI) ions. The study lasted for 100 min and was carried out at a pH of 6. Improving the adsorption capability of Cr(VI) ions onto the material was the main goal of this experimental setup. The absorbent that accumulates Cr(VI) ions was then submerged in a 50 mL solution of 0.05 mol L^{-1} ethylenediaminetetraacetic acid (EDTA) after the filtration process. For four hours, the mixture was continuously stirred at a carefully regulated temperature of 298.15 K. The purpose of this procedure was to promote the desorption process by improving the contact between the absorbent material and the EDTA solution. After this phase, the main technique used to extract the TACGC from its composite matrix was centrifugation. Afterward, a washing phase applying distilled water was implemented to guarantee the removal of impurities. After this cleaning process, the membrane was subjected to drying under vacuum conditions at a precisely regulated temperature of 333 K, which prepared it for reintegration in the following cycle. Five thorough iterations of the adsorption and reactivation processes were carried out. One important feature of the sorbent that highlights its usefulness for possible commercial applications is its remarkable reactivation capability.[62,63] Retention capacities were significantly reduced during the course of five consecutive cycles of

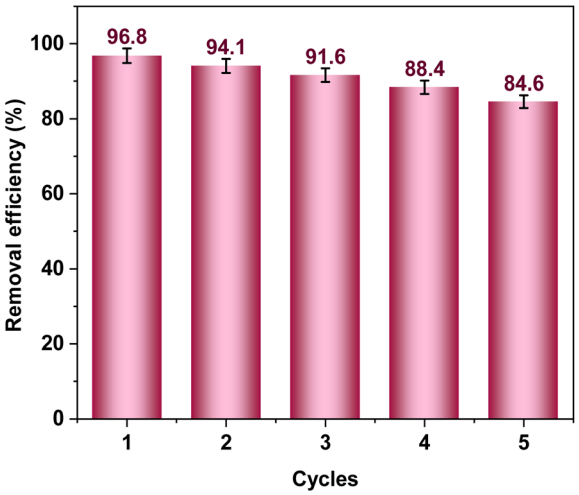

Fig. 11 The reusability of TACGC.

adsorption and desorption, providing values of 96.8, 94.1, 91.6, 88.4, and 84.6% of the starting capacity for each cycle, respectively. This steady decrease in uptake can be attributed to the material's changing geometric structure and active site depletion, which become more noticeable with each cycle repetition. The TACGC exhibits effective performance for up to five cycles, as shown in Fig. 11. This finding implies that the adsorbent consistently maintains its stability over the course of the testing. The findings suggest that the TACGC has significant potential for efficient recycling processes. XRD analysis was carried out both before and after the regeneration process to assess the stability of the TACGC, as depicted in Fig. S2(a). The research shows that even after five regeneration cycles, the adsorbent's structural integrity is unaffected.[64–66] The FT-IR spectra of fresh and regenerated TACGC show that the composite sponge retains structural integrity after multiple cycles of Cr(VI) removal, indicating chemical stability. Both samples exhibit a broad band at 3300–3400 cm^{-1} related to O–H and N–H stretching from hydroxyl, carboxyl, and amine groups in the GG–CMC–IA polymer and activated carbon surface, suggesting functional group stability post-regeneration. Peaks near 2900 cm^{-1} demonstrate minimal intensity reductions, indicating preserved functionality. The C=O stretching region (1650 to 1720 cm^{-1}) remains intact, with minor intensity shifts due to chromium complexation. The fingerprint region (1000–1200 cm^{-1}) shows C–O–C stretching and polysaccharide backbone vibrations in both samples, confirming GG–CMC integrity. The regenerated TACGC displays slightly increased transmittance, indicating effective Cr species removal *via* EDTA washing. The absence of new peaks confirms no irreversible chemical reactions or degradation, reaffirming TACGC's functional group retention, structural stability, and reusability (Fig. S2(b)). The SEM micrograph of the regenerated TACGC composite shows that it retains its unique porous and interconnected sponge-like structure after multiple adsorption–desorption cycles, demonstrating significant morphological stability. Its surface features a diverse arrangement of micro- and mesopores, with irregular rough areas, indicating that the

polymer-carbon framework remains intact during interactions with Cr(VI) and the EDTA regeneration solution. While slight surface smoothing and small fissures are present, likely from chromium deposition and removal, the pore channels are unobstructed, ensuring efficient mass transfer. The absence of extensive collapsed regions confirms that the GG–CMC–IA matrix protects the TAC particles from structural degradation. Additionally, the maintained rough texture and visible fracture lines indicate that active sites for chromium binding are still available. Overall, these results demonstrate that TACGC possesses outstanding regeneration stability, keeping its porous structure and functionality, thus improving its reusability for Cr(VI) removal applications (Fig. S2(c)).

3.11. In contrast to other adsorbents

Table S9 offers a comprehensive qualified study of the performance characteristics of the synthesized adsorbent concerning its efficacy in adsorbing various substances aimed at the removal of Cr(VI), as reported in the relevant academic literature. The results indicate significant variations in the maximum adsorption capacities of the materials evaluated. The findings show that the materials' greatest absorption capabilities varied significantly. Particularly, the developed adsorbent exhibited enhanced performance, achieving an experimental maximum capacity of $q_{max} = 404.87$ mg g^{-1}. This finding underscores its potential as an effective and practical intermediate solution for Cr(VI) removal.

3.12. Statistical study

3.12.1. ANOVA. The conducted analysis of variance (ANOVA) regarding the adsorption of Cr(VI) onto the TACGC reveals a statistically significant overall model. This conclusion is supported by a noteworthy *F*-value of 57.77, accompanied by a *P*-value that is less than 0.0001.[2] According to the results, the model effectively illustrates the relationship between the independent factors and the response with regard to Cr(VI) adsorption. A detailed analysis of the linear factors reveals that the adsorbent dose (*B*) exerted the most substantial influence, evidenced by an *F*-value of 312.52 and a *P*-value less than 0.0001. Additionally, contact time (*C*) and pH (*A*) emerged as statistically significant variables, with *P*-values of 0.0003 and 0.0143, individually. The interaction between dose and time (BC) was significant ($P = 0.0130$), indicating a collaborative effect of these parameters, while the interactions involving pH (AB and AC) did not show significant results ($P > 0.05$), suggesting limited combined impact. The quadratic components A^2 and B^2 exhibited a notable level of significance ($P = 0.0004$ and < 0.0001, individually), which suggests the attendance of nonlinear influences of pH and amount on the adsorption mechanism. In contrast, the quadratic term associated with time (C^2) did not reach significance ($P = 0.5924$), implying that a linear relationship is maintained throughout the evaluated duration. The coefficient of determination ($R^2 = 0.9867$), adjusted R^2 (0.9696), and predicted R^2 (0.7874) designate a strong fit of the model and its predictive capability. Furthermore, the precision value of 25.6017 exceeds the established threshold, thereby validating an acceptable signal-to-noise ratio.[1] The relatively low standard deviation (18.32) and coefficient of variation (8.36%) suggest good reproducibility and reliability of the model. However, the equality of the lack of fit value to the total residual implies that model enhancement or the addition of more replicate experiments could further refine the findings. In summary, the ANOVA results substantiate the model's robustness and efficiency in representing the Cr(VI) adsorption behavior on the TACGC (Table 2).

The information illustrated in Table 3 shows that the quadratic model demonstrates superior efficacy in accurately

Table 2 The models used have undergone a comprehensive study of variance

Source	Sum of squares	d*f*	Mean squares	*F*-value	*P*-value	
Model	1.744×10^5	9	19 380.19	57.77	<0.0001	Significant
A-pH	3513.62	1	3513.62	10.47	0.0143	
B-dose	1.049×10^5	1	1.049×10^5	312.52	<0.0001	
C-time	14 490.61	1	14 490.61	43.19	0.0003	
AB	768.77	1	768.77	2.29	0.1739	
AC	545.73	1	545.73	1.63	0.2429	
BC	3674.50	1	3674.50	10.95	0.0130	
A^2	13 080.83	1	13 080.83	38.99	0.0004	
B^2	30 566.84	1	30 566.84	91.11	<0.0001	
C^2	105.55	1	105.55	0.3146	0.5924	
Residual	2348.50	7	335.50			
Lack of fit	2348.50	3	782.83			
Pure error	0.0000	4	0.0000			
Cor. total	1.768×10^5	16				
Std. dev.	18.32					
Mean	219.12					
C.V. %	8.36					
R^2	0.9867					
Adjusted R^2	0.9696					
Predicted R^2	0.7874					
Adeq precision	25.6017					

Table 3 The total sum of squared deviations for the following models

Source	Sum of squares	d*f*	Mean square	Sequential *p*-value	Adjusted R^2	Predicted R^2	
Linear	53 914.74	9	5990.53	0.0012	0.6246	0.4902	
2FI	48 925.73	6	8154.29	0.7971	0.5572	0.1129	
Quadratic	2348.48	3	782.83	<0.0001	0.9696	0.7874	Suggested
Cubic	0.0000	0			1.0000		Aliased

representing the adsorption characteristics of Cr(VI) on the TACGC. The linear model demonstrated a notable level of statistical significance, demonstrated by a sequential *p*-value of 0.0012. However, the accompanying fit statistics were only moderate in nature, with an adjusted R^2 of 0.6246 and a Predicted R^2 of 0.4902. These values suggest a restricted capability of the model to elucidate and forecast the outcomes effectively. In contrast, the two-factor interaction (2FI) model exhibited even poorer performance, reflected by a non-significant *p*-value of 0.7971 and lower fit metrics, yielding an adjusted R^2 of 0.5572 and a predicted R^2 of 0.1129. This further underscores the inadequacy of the 2FI model in taking the underlying patterns of the data. The inclusion of interaction terms seems to have failed in improving the model's performance, contributing instead to increased complexity without clear benefit. Conversely, the quadratic model exhibited a highly noteworthy *p*-value below 0.0001, accompanied by robust adjusted R^2 (0.9696) and predicted R^2 (0.7874) metrics. These values reflect a strong correspondence between the model's accuracy and its predictive capability. This robust statistical performance reinforces the notion that the quadratic model effectively captures the nonlinear relationships influencing Cr(VI) removal. While the cubic model may theoretically provide a more nuanced representation, its practicality is compromised by an insufficient number of degrees of freedom. Therefore, the quadratic model appears as the most appropriate and statistically valid option for subsequent analyses and process optimization.[6]

The expression defined through coded variables allows the estimating of the answer consistent to designated levels of each variable. In this framework, elevated levels of the variables are typically indicated by +1, whereas reduced levels are represented by −1.[6] The coded equation serves an important function in assessing the relative impact of various issues. It facilitates the analysis of the coefficients linked to each factor, as demonstrated in eqn (4):

$$q_e = 287.806 + 20.9573 \times A - 42.5614 \times B + 114.484 \times C - 11.6804 \times AB + 13.863 \times AC - 30.3055 \times BC - 55.7358 \times A^2 - 5.0087 \times B^2 - 85.2049 \times C^2 \quad (4)$$

The equation, when applied to the relevant variables, functions as a forecasting instrument that predicts responses based on designated values for individually variable. For each variable, these values must be stated in their original units. However, because the coefficients in this equation have been standardized to match the units of the corresponding variables, it is not sufficient to assess the relative importance of the various variables. Moreover, the intercept does not correspond to the central location within the design space, as demonstrated in eqn (5).

$$q_e = -124.176 + 68.025 \times pH + 88.5571 \times dose + 6.58017 \times time - 16.2228 \times pH\ dose + 0.0972842 \times pH\ time - 2.65837 \times dose\ time - 6.19287 \times pH^2 - 86.9566 \times dose^2 - 0.0377639 \times time^2 \quad (5)$$

Fig. 12(a) offerings a normal probability plot of the residuals, which serves as a diagnostic tool to evaluate whether the errors from the regression model adhere to a normal distribution. This adherence is crucial for ensuring the validity of ANOVA and regression analyses. In this plot, the externally studentized residuals are plotted against their respective normal probability values. The data points exhibit a significant correlation with the red diagonal reference line, suggesting that the residuals are roughly distributed in a manner conforming to a normal distribution. There are no significant deviations or outliers visible, and the residuals exhibit a symmetrical distribution around zero. This advises that the discrepancies within the model are both random and impartial. This alignment strengthens the statistical dependability of the regression model utilized for Cr(VI) adsorption on the TACGC, confirming that the foundational assumptions of the model hold true and that the fitted model upholds its statistical validity.[7]

3.12.2. Experimental design modeling and response surface analysis. A crucial diagnostic tool for assessing the accuracy and predictive power of the regression model used to evaluate Cr(VI) adsorption on the TACGC is Fig. 12(b), which compares anticipated values with actual results.[67,68] In this graphical representation, the *x*-axis displays the actual experimental values, whereas the *y*-axis illustrates the predicted values formed by the model. The closeness of the data points to the 45° diagonal line signifies a robust correlation between the observed and predicted results. This close alignment verifies that the model effectively forecasts Cr(VI) removal across the range of experiments, with only slight deviations. The absence of notable outliers or discernible patterns implies that the model is neither underfitting nor overfitting and successfully captures the primary trends within the data. This graphical verification reinforces the high R^2 and adjusted R^2 values obtained in the ANOVA analysis, further highlighting the model's robustness and its appropriateness for optimization and process prediction regarding heavy metal adsorption.[10]

Fig. 12(c) exemplifies a Box–Cox plot working for the purpose of power transformations, which serves to determine the most appropriate power transformation for the answer variable. This approach is intended to stabilize alteration and improve the

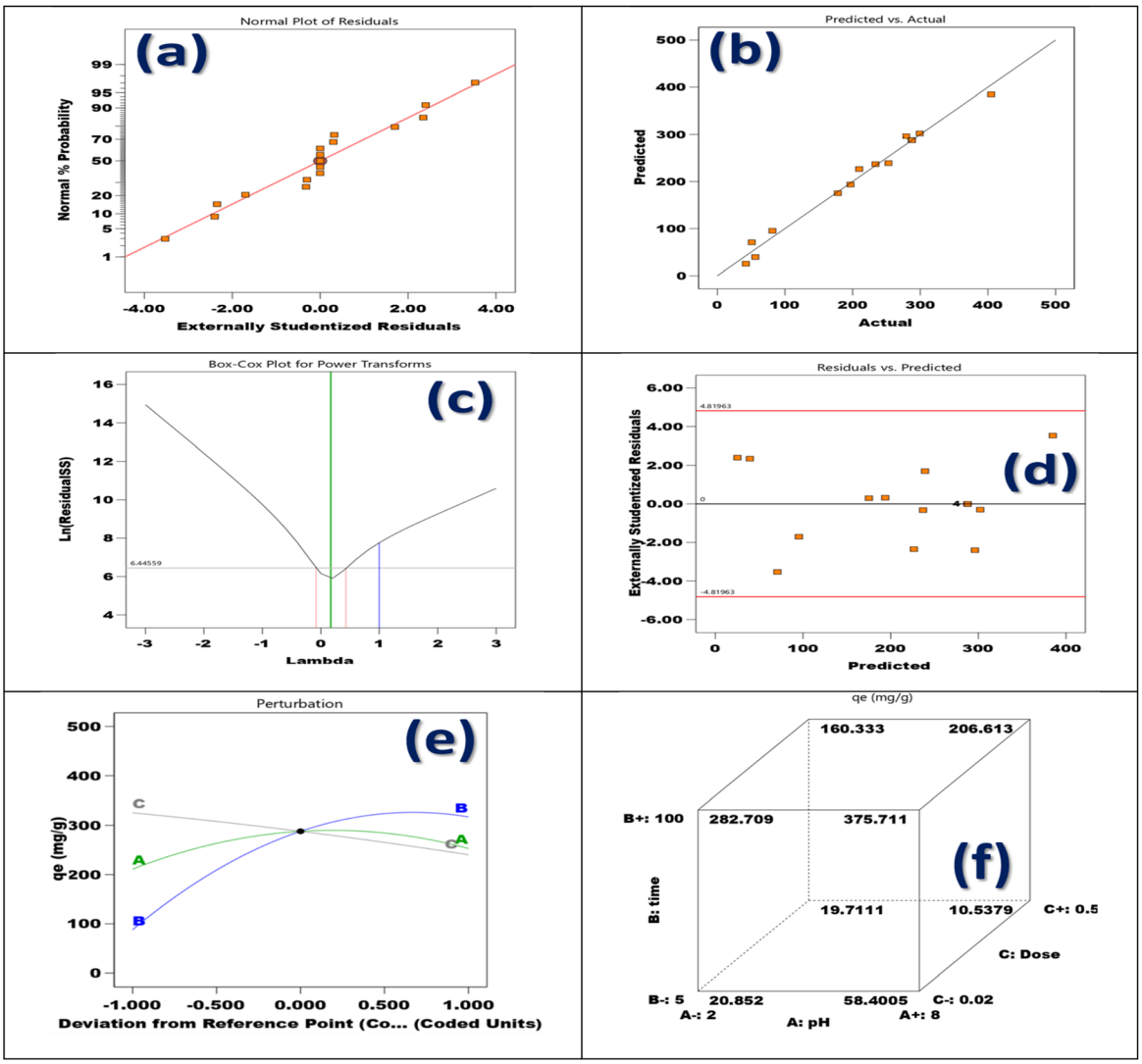

Fig. 12 (a) A normal % probability plot which assesses the distribution of a dataset, (b) a comparison of predicted values against actual outcomes, (c) a Box–Cox plot illustrating power transformations applicable to Cr(VI), (d) a visual of extremely standardized residuals plotted against predicted values, (e) a perturbation plot demonstrating the effect of varying input parameters, and (f) a depiction of cubic interactions indicating nonlinear relationships among variables.

regularity of residuals in the context of regression analysis concerning Cr(VI) adsorption facilitated by the TACGC composite sponge. The graph presents the normal logarithm of the remaining number of squares (Ln (Residual SS)) plotted along the *y*-axis, while multiple lambda (λ) values are represented on the *x*-axis. Notably, the vertical green line marks the optimal λ value, which approaches zero. This observation implies that applying a logarithmic transformation to the response variable may yield the most advantageous outcome. The red and blue vertical lines denote the 95% confidence interval for lambda, indicating that transformations within this range do not substantially degrade the model fit. The $\lambda = 0$ value, which resides within this confidence interval and correlates with the minimum residual sum of squares, suggests that either no further transformation is necessary or a log transformation is adequate. This observation strengthens the strength of the model's structure and bolsters the statistical premises concerning the uniformity of variance as well as the normality of residual distributions.[69,70]

Fig. 12(d), depicting the residuals *vs.* predicted plot, serves as a diagnostic tool to evaluate the assumptions related to homoscedasticity, which pertains to the uniform variance of residuals. This plot also aids in detecting potential outliers or emerging patterns that could indicate inaccurate model specifications in the analysis of Cr(VI) adsorption using the TACGC. In this plot, externally studentized residuals are represented on the *y*-axis, while predicted values are plotted on the *x*-axis. Ideally, these residuals should be randomly and symmetrically distributed around the zero line, without displaying any discernible trends or patterns. The data points in this particular plot are relatively evenly spread around the horizontal zero line, and all residuals remain comfortably within the red control

limits (±4.81963), which suggests the absence of significant outliers. Additionally, there is no indication of funnel shapes or curvature, which points to a constant variance of residuals across the predicted value spectrum. This confirms that the model adheres to the homoscedasticity assumption, and the residuals exhibit expected behavior. The gathered evidence strongly supports the model's reliability and its efficiency in precisely representing the adsorption behavior of Cr(VI) on the TACGC.[71,72]

Fig. 12(e) features a perturbation plot that illustrates the responsiveness of the Cr(VI) adsorption capacity (q_e), quantified in mg g^{-1}, to alterations in three defined process variables: *A* (pH), *B* (adsorbent dose), and *C* (contact time), while holding all other factors constant at a reference level. The individual curves presented on the plot depict the variation in the response variable as one specific factor shifts from its mean (reference) position. The analysis reveals that factor *B* (adsorbent dose), indicated by the blue curve, demonstrates the most significant curvature and steep gradient, signifying its strong impact on Cr(VI) adsorption. As the adsorbent dose increases from a low level, the adsorption capacity rises rapidly, reaches a peak, and then shows a slight decline at higher doses, indicating a nonlinear response and a potential saturation effect. Factor *A* (pH), represented by the green curve, also plays an important role in adsorption, displaying an increasing trend that eventually levels off, which suggests the presence of an optimal pH range for achieving maximum adsorption efficiency. In contrast, factor *C* (contact time), depicted by the gray curve, illustrates a nearly horizontal line, indicating that, within the examined range, contact time has a relatively minor influence on adsorption capacity. This analysis further corroborates the ANOVA results, highlighting that dose and pH are essential parameters, while contact time plays a less significant role under the conditions tested. The plot effectively visually reinforces the predominance of adsorbent dose (*B*) in optimizing the removal of Cr(VI) using the TACGC.[73,74]

The 3D cube plot (Fig. 12(f)) illustrates the interactive effects of pH (*A*), contact time (*B*), and adsorbent dose (*C*) on the capacity for Cr(VI) adsorption (q_e, mg g^{-1}) using the TACGC composite sponge. Each axis represents the varying levels of these parameters. The maximum adsorption capacity recorded is 375.711 mg g^{-1}, occurring under specific conditions that include a high pH level of 8, an extended contact duration of 100 min, and a minimal amount of adsorbent utilized, quantified at 0.02 g.[75–77] This suggests that alkaline conditions coupled with sufficient interaction time greatly improve Cr(VI) uptake, especially when the sponge's active sites are not fully saturated. Conversely, the lowest adsorption capacity recorded was 10.5379 mg g^{-1}, happening at high pH, with a short interaction time (5 min), and a high adsorbent dose (0.5 g). This reduction in capacity can be accredited to the aggregation of active places at higher dosages, which decreases the effective surface area and restricts accessibility to Cr(VI). The plot also indicates that at low pH (2) and minimal dosages, adsorption remains low regardless of contact time, underscoring the adverse effects of acidic conditions on Cr(VI) removal. These observations underscore the necessity of optimizing all three variables collectively and reinforce findings from the ANOVA and perturbation analysis, highlighting that the adsorbent dose is the most sensitive variable, while pH and time also significantly contribute to the enhancement of adsorption capacity in the TACGC.[15]

3.12.3. Model adequacy checking. A contour plot, a desirability plot, and a three-dimensional interaction surface are the three different visual representations shown in Fig. 13(a). Collectively, these visualizations illustrate the effect of two variables adsorbent amount (*A*) and communication time (*B*) on the adsorption capacity of Cr(VI) (q_e, expressed in mg g^{-1}) utilizing the TACGC, all while keeping the pH level consistent. Analysis of the 3D surface plot reveals an evident downward trend, suggesting that an increase in adsorbent amount correlates with a important decrease in adsorption capacity, whereas an extended contact time has a positive effect, enhancing the adsorption capability. The supreme adsorption capacity, approximately 400 mg g^{-1}, is recorded at a minimal dosage of approximately 0.02 g combined with a prolonged contact duration of around 100 min. In contrast, the minimal adsorption capability of roughly 42 mg g^{-1} is noted at a higher dosage of 0.5 g with a significantly shorter contact time of only 5 min. This evidence illustrates an inverse correlation between dosage and equilibrium adsorption capacity (q_e), potentially attributable to phenomena such as site aggregation or a diminished driving force for adsorption.[78–80] The contour plot reinforces this trend from a top-down perspective, indicating that the upper left area (characterized by low dose and longtime) corresponds to high adsorption capacity (marked in red), while the lower right area (defined by high dose and short time) is associated with low q_e (shown in blue). Additionally, the desirability plot identifies the optimal conditions for maximizing Cr(VI) removal efficiency, with desirability values growing towards the upper left area, achieving a peak of 0.970. This indicates that the ideal conditions for adsorption are characterized by minimal dosages and extended contact times, thereby optimizing the balance between effective adsorption performance and resource efficiency.[17]

Fig. 13(b) presents three distinct graphical formats: a 3D surface plot, a contour plot, as well as a desirability plot, all of which underscore the interactive effects of pH (*A*) and adsorbent dosage (*B*) on the adsorption capacity (q_e, mg g^{-1}) of Cr(VI) when utilizing the TACGC. The 3D interaction plot features a dome-shaped surface, highlighting a notable correlation between q_e and the variables of pH and adsorbent amount. The capacity for adsorption increases as the pH level rises, peaking at an optimal point near pH 5. Beyond this threshold, there is a marginal reduction in adsorption efficiency. Conversely, a higher dosage of adsorbent generally leads to a reduction in q_e, likely due to potential overlapping of particles and diminished surface area availability. This occurrence is distinctly illustrated in the contour plot, which reveals that the peak adsorption capacity (approximately 300 mg g^{-1}) emerges at around pH 5 and a minimal dosage (approximately 0.02 g), as denoted by the yellow region. The desirability plot also affirms this optimal zone, recording the highest desirability value (0.970) at low dosage and pH values between 4.5 and 5.0, with a decline

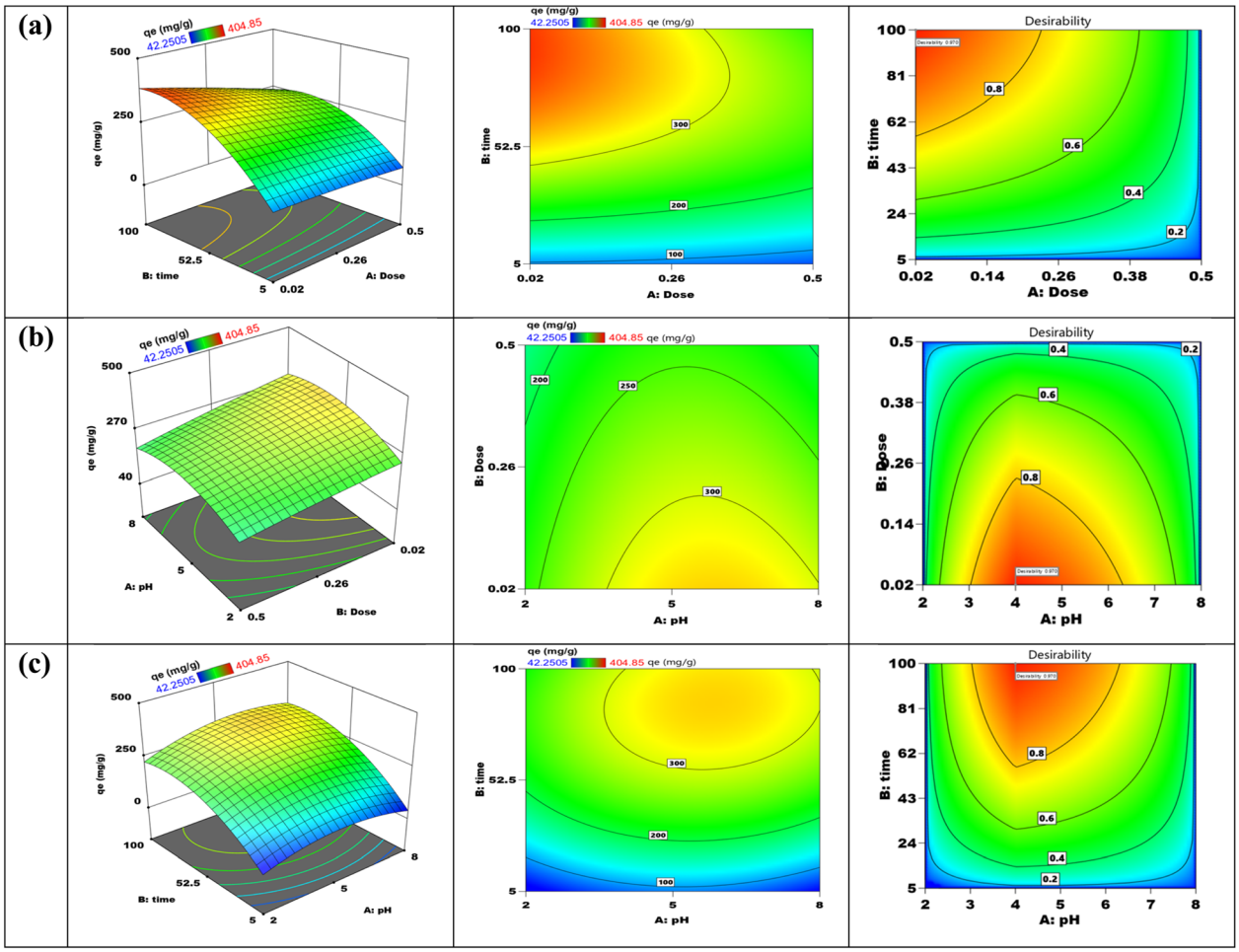

Fig. 13 Contour and 3D interaction between Cr(VI) and TACGC (a) interaction between dose and time, (b) dose and pH, and (c) pH and time.

observed when either the dosage increases or the pH moves away from the optimal range. These findings indicate that conditions of moderate acidity combined with minimal adsorbent loading are most effective for enhancing Cr(VI) adsorption, highlighting the importance of electrostatic interactions and optimal utilization of active sites in this process.[17]

Three distinct visual formats a contour plot, a desirability plot, and a three-dimensional surface plot are depicted in Fig. 13(c). Together, these illustrations show how pH (A) and contact duration (B) interact to affect the Cr(VI) adsorption capacity (q_e, expressed in mg g^{-1}) when the TACGC composite sponge is used and the adsorbent dose is kept constant. The three-dimensional surface plot distinctly portrays an upward-curving surface, suggesting that the adsorption capability (q_e) increases with both pH and communication time. It reaches its maximum at around pH 5 and a contact extent of 100 min, after which the adsorption capacity stabilizes. This reflection is corroborated by the contour plot, which identifies the highest q_e values (above 300 mg g^{-1}) in the upper-central region of the graph, where contact time is maximized and pH hovers around 5. Variations from the ideal pH, whether they involve lower or higher values in conjunction with decreased contact times, are linked to a notable reduction in the quantity adsorbed per gram (q_e). This pattern implies that extended contact durations enhance the diffusion of ions and strengthen the interactions with the active sites present. Furthermore, a moderately acidic pH is advantageous as it encourages electrostatic attraction between Cr(VI) ions and the surface of the composite sponge. The desirability plot further reinforces this optimal range, revealing that the peak desirability score of 0.970 is attained at a pH near 4.5 to 5, alongside a maximum contact duration of approximately 100 min. These results underscore the importance of sufficient contact time and an appropriate pH range in attaining optimal Cr(VI) removal, consistent with considerations regarding kinetics and surface charge.[19]

3.12.4. The validation of models and the desirability strategy. The ramp plots illustrated in Fig. 14(a) effectively delineate the individual impacts of adsorbent amount (A), communication time (B), and pH (C) on achieving an optimal overall desirability score of 0.970 for the Cr(IV) adsorption through the TACGC, as well as the estimated adsorption capacity (q_e). In the upper-left plot, the adsorbent dose (A) is systematically altered from 0.02 to 0.50 g. The red marker positioned near the 0.02 g dosage indicates that this minimal quantity produces the greatest desirability. This phenomenon can be attributed to the lower sponge loading, which mitigates

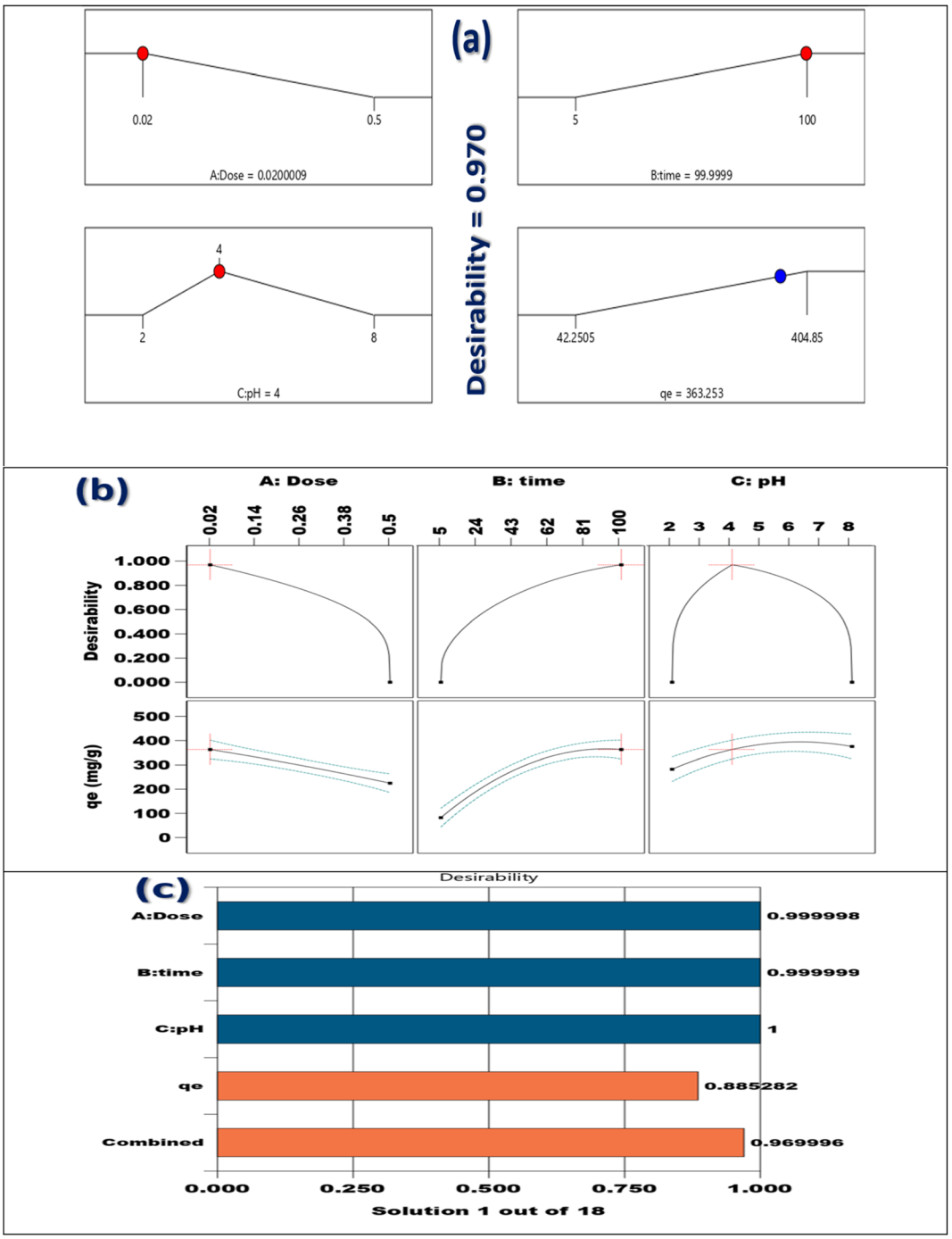

Fig. 14 (a) Growing curiosity about the best numerical solutions, (b) desirability of every answer, and (c) an individual desirability bar graph is displayed.

site aggregation and enhances the adsorption efficacy (q_e) relative to the mass of the adsorbent. The upper-right plot indicates that the contact time (B) ranges from 5 to 100 min, with the red marker positioned at 100 min, suggesting that extended interaction periods enhance removal efficiency, allowing Cr(VI) ions to fully diffuse and attach to the active sites. The lower-left graph depicts fluctuations in pH (C) ranging from 2 to 8. A moderately acidic environment promotes advantageous electrostatic relationships involving negatively charged Cr(VI) ions and the positively charged functional groups found on the composite surface, as seen by a red indication at pH 4. Notably, the effectiveness of these interactions decreases as pH levels surpass 4. Lastly, the lower-right plot represents the predicted q_e (mg g^{-1}) across a range from 42.25 to 404.85, with a blue marker at 363.25 mg g^{-1}, which corresponds to the model's predicted adsorption capacity under the optimal conditions ($A = 0.02$ g, $B = 100$ min, $C = 4$). Collectively, these plots illustrate that the ideal strategy for achieving near-complete Cr(VI) elimination

involves employing the lowest dose, the longest contact time, and a pH of 4, thereby maximizing both the predicted q_e and overall desirability.[64]

Fig. 14(b) offerings a comprehensive optimization analysis of the adsorption process of Cr(VI) onto the TACGC. This analysis investigates the individual effects of three key variables: adsorbent dosage (A), communication time (B), and pH level (C) on two critical outcomes: overall desirability, depicted in the better section of the figure, and adsorption capability (q_e, measured in mg g^{-1}), illustrated in the lower section. The desirability plots indicate that the most promising situations for adsorption occur at a minimal amount of 0.02 g of adsorbent, a contact length of 100 min, and a pH around 4, as denoted by the peak values highlighted with red crosses. Notably, desirability declines significantly with increasing adsorbent dose due to diminished surface efficiency and potential particle aggregation. In contrast, desirability improves with extended contact time as equilibrium is approached, and it demonstrates a bell-shaped relationship concerning pH, emphasizing the significance of electrostatic attraction around a pH of 4. Correspondingly, the q_e plots illustrate these patterns: adsorption capacity diminishes as the dose increases, increases with time until it levels off at equilibrium, and peaks around pH 4 to 5. The presence of narrow confidence intervals (depicted by dashed lines) surrounding these curves further validates the model's predictions. Overall, this analysis verifies that employing a low adsorbent dose, prolonged contact time, and suitable pH levels collectively enhance both adsorption capacity and desirability of the process, establishing these parameters as optimal for maximizing Cr(VI) removal efficiency.[13]

Fig. 14(c) presents a desirability bar diagram that effectively summarizes the results of the optimization process involving the adsorption of Cr(VI) on the TACGC. This analysis is grounded in the specified input parameters and corresponding response metrics. The chart breaks down the desirability scores associated with three critical factors: amount (A), contact time (B), and pH (C), together with the response variable, q_e (adsorption capability), culminating in a comprehensive overall desirability score. The desirability values for the dose (0.999998), contact time (0.999999), and pH (1.000000) are all exceptionally close to 1, suggesting that the chosen operating conditions (0.02 g dose, 100 min of contact time, and pH 4) are nearly optimal for achieving the desired operational targets. The predicted adsorption capacity (q_e) has a somewhat lower desirability score of 0.885282, indicating a high-performance result while revealing a slight compromise relative to the theoretical maximum. The overall combined desirability value of 0.969996 further verifies that the optimized conditions create a nearly ideal equilibrium among all process variables, facilitating highly efficient Cr(VI) removal. This outcome underscores the effectiveness and reliability of the multi-criteria optimization strategy implemented in this research.[13]

4. Conclusion

The research findings indicate that the TACGC composite sponge serves as a strong, sustainable, and highly effective bioadsorbent for the extraction of Cr(VI) from water sources. This composite is created by combining tobacco-derived activated carbon with a biodegradable dual-polymer matrix consisting of guar gum and carboxymethyl cellulose, which is crosslinked with itaconic acid. This design not only enhances mechanical stability and surface functionality but also adheres to green chemistry principles by utilizing inexpensive, renewable materials and waste biomass. The composite demonstrates a high adsorption capacity, swift kinetics, and favorable thermodynamic properties, representative that the procedure of Cr(VI) uptake is both spontaneous and endothermic, primarily driven by electrostatic interactions and surface complexation. Furthermore, the material shows significant reusability, maintaining its effectiveness across five consecutive regeneration cycles, which emphasizes its economic and practical viability. Statistical optimization *via* the Box–Behnken design has further validated the reliability and efficiency of the process under different operational conditions, providing a predictive framework for large-scale applications. Overall, these results highlight the TACGC as a promising bio-based solution for advanced industrial or municipal wastewater treatment, with important implications for developing environmentally friendly and industrially applicable technologies for the remediation of heavy metals.

Conflicts of interest

The authors declare that they have no known competing financial interests or personal relationships that could have appeared to influence the work reported in this paper.

Data availability

The data that support the findings of this study are available from the corresponding author upon reasonable request.

Supplementary information (SI) is available. See DOI: https://doi.org/10.1039/d5ra07331f.

Acknowledgements

This work was supported and funded by the Deanship of Scientific Research at Imam Mohammad Ibn Saud Islamic University (IMSIU) (grant number IMSIU-DDRSP2502).

References

1 H. Hadiyanto, M. Christwardana, W. Widayat, A. K. Jati and S. I. Laes, Optimization of flocculation efficiency and settling time using chitosan and eggshell as bio-flocculant in Chlorella pyrenoidosa harvesting process, *Environ. Technol. Innovation*, 2021, **24**, 101959.

2 H. S. Kusuma, A. N. Amenaghawon, H. Darmokoesoemo, Y. A. Neolaka, B. A. Widyaningrum, S. U. Onowise and C. L. Anyalewechi, A comparative evaluation of statistical empirical and neural intelligence modeling of Manihot esculenta-derived leaves extract for optimized bio-

coagulation-flocculation of turbid water, *Ind. Crops Prod.*, 2022, **186**, 115194.

3 S. R. Soomro, S. N. Soomro, S. Syed, S. Hassan, and B. Tabassum, Cotton stalks: potential biofuel recourses for sustainable environment, *Biotechnology and Omics Approaches for Bioenergy Crops*, Springer2023, pp. , pp. 203–234.

4 A. S. Martins-da-Silva, J. Torales, R. F. V. Becker, H. F. Moura, M. Waisman Campos, T. M. Fidalgo, A. Ventriglio and J. M. Castaldelli-Maia, Tobacco growing and tobacco use, *Int. Rev. Psychiatr.*, 2022, **34**, 51–58.

5 G. Manthos and K. Tsigkou, Upscaling of tobacco processing waste management: A review and a proposed valorization approach towards the biorefinery concept, *J. Environ. Manage.*, 2025, **387**, 125942.

6 H. S. Kusuma, A. Ansori, S. Wibowo, D. S. Bhuana and M. Mahfud, Optimization of transesterification process of biodiesel from Nyamplung (Calophyllum inophyllum Linn) using microwave with CaO catalyst, *Korean Chem. Eng. Res.*, 2018, **56**, 435–440.

7 A. I. Khuri and S. Mukhopadhyay, Response surface methodology, *Wiley Interdiscip. Rev. Comput. Stat.*, 2010, **2**, 128–149.

8 A. K. Das, M. S. Saikh, A. Misra, M. S. Ali, P. Pradhan, N. Sepay, S. Dhibar, M. Afzal, S. J. Abbas and N. Sepay, Heterogeneous Nickel Nanoparticles Catalysed Ligand-Free Hydroxylation of Aryl halides in Aqueous Medium and DFT Investigation, *J. Mol. Struct.*, 2025, **1352**, 144012.

9 A. Das, D. Chavda, M. Manna and A. K. Das, Dual-active Hf (iv)–organic framework for the detection of FOX-7 and as a heterogeneous catalyst for Knoevenagel condensation, *New J. Chem.*, 2024, **48**, 18249–18260.

10 A. H. Jawad and S. Surip, Upgrading low rank coal into mesoporous activated carbon via microwave process for methylene bluedye adsorption: Box Behnken Design and mechanism study, *Diamond Relat. Mater.*, 2022, **127**, 109199.

11 H. Kusuma, M. Syahputra, D. Parasandi, A. Altway and M. Mahfud, Optimization of microwave hydrodistillation of dried patchouli leaves by response surface methodology, *Rasayan J. Chem.*, 2017, **10**, 861–865.

12 A. Latif, A. Maqbool, R. Zhou, M. Arsalan, K. Sun and Y. Si, Optimized degradation of bisphenol A by immobilized laccase from Trametes versicolor using Box-Behnken design (BBD) and artificial neural network (ANN), *J. Environ. Chem. Eng.*, 2022, **10**, 107331.

13 K. Aziz, F. Aziz, R. Mamouni, L. Aziz and N. Saffaj, Engineering of highly Brachychiton populneus shells@ polyaniline bio-sorbent for efficient removal of pesticides from wastewater: Optimization using BBD-RSM approach, *J. Mol. Liq.*, 2022, **346**, 117092.

14 A. K. Das, M. S. Ali, A. Misra, S. Islam, B. Kar, S. Biswas, G. Ghatak, D. Mal, M. Shit and M. Dolai, Green Synthesized Biogenic Ag Nanoparticles With Enhanced Antibacterial, Antifungal, Antibiofilm, and Antioxidant Activities: Catalytic Applications in the ipso-Hydroxylation of Aryl Boronic Acids, *Appl. Organomet. Chem.*, 2025, **39**, e7796.

15 M. Reji and R. Kumar, Response surface methodology (RSM): An overview to analyze multivariate data, *Indian J. Microbiol. Res*, 2022, **9**, 241–248.

16 A. K. Das, A. Misra, M. S. Ali, M. S. Saikh, S. Dhibar, K. K. Banerjee, G. Ghatak, D. Mal, M. Shit and S. Biswas, Investigating the potent antibacterial, antibiofilm, antidiabetic, and antioxidant activities of biosynthesized iron oxide nanoparticles: recyclable catalyst for ammoxidation of aromatic aldehydes, *RSC Adv.*, 2025, **15**, 35844–35858.

17 A. H. Jawad, U. K. Sahu, M. S. Mastuli, Z. A. ALOthman and L. D. Wilson, Multivariable optimization with desirability function for carbon porosity and methylene blue adsorption by watermelon rind activated carbon prepared by microwave assisted H3PO4, *Biomass Convers Biorefin.*, 2022, 1–15.

18 A. Das and A. K. Das, A functionalized Hf (iv)–organic framework introducing an efficient, recyclable, and size-selective heterogeneous catalyst for MPV reduction, *New J. Chem.*, 2023, **47**, 5347–5355.

19 S. Roy, A. K. Saha, S. Panda and G. Dey, Optimization of turmeric oil extraction in an annular supercritical fluid extractor by comparing BBD-RSM and FCCD-RSM approaches, *Mater. Today: Proc.*, 2023, **76**, 47–55.

20 J. Sreńscek-Nazzal, J. Serafin, A. Kamińska, A. Dymerska, E. Mijowska and B. Michalkiewicz, Waste-based nanoarchitectonics with face masks as valuable starting material for high-performance supercapacitors, *J. Colloid Interface Sci.*, 2022, **627**, 978–991.

21 A. C. Gonçalves Jr, J. Zimmermann, D. Schwantes, V. H. D. de Oliveira, F. da Cunha Dudczak, C. R. T. Tarley, M. C. Prete and A. Snak, Recycling of tobacco wastes in the development of ultra-high surface area activated carbon, *J. Anal. Appl. Pyrolysis*, 2023, **171**, 105965.

22 Z. Wardighi, A. E. Amri, L. Kadiri, A. Jebli, F. Z. Bouhassane and A. Lebkiri, Ecological study of elimination of the organic pollutant (violet crystal) using natural fibers of Rubia tinctorum: Optimization of adsorption processes by BBD-RSM modeling and DFT approaches, *Inorg. Chem. Commun.*, 2023, **155**, 111014.

23 K. Aziz, R. Mamouni, A. Azrrar, B. Kjidaa, N. Saffaj and F. Aziz, Enhanced biosorption of bisphenol A from wastewater using hydroxyapatite elaborated from fish scales and camel bone meal: A RSM@ BBD optimization approach, *Ceram. Int.*, 2022, **48**, 15811–15823.

24 C. Qiu, H. Sun, Y. Ni, Z. Dou, M. Xia, Z. Fei, Z. Zhang, M. Cui, Q. Liu and X. Qiao, Removal of tetracycline by La (OH) 3 modified MIL-101 (Cr) adsorbent with multiple adsorption sites, *Mater. Today Commun.*, 2024, 109613.

25 R. Nazerifard, M. Mohammadpourfard and S. Z. Heris, Optimization of the integrated ORC and carbon capture units coupled to the refinery furnace with the RSM-BBD method, *J. CO_2 Util.*, 2022, **66**, 102289.

26 R. Venkatraman and S. Raghuraman, Experimental analysis on density, micro-hardness, surface roughness and processing time of Acrylonitrile Butadiene Styrene (ABS) through Fused Deposition Modeling (FDM) using Box

Behnken Design (BBD), *Mater. Today Commun.*, 2021, **27**, 102353.

27 A. Afzalinia, M. Mirzaee and M. A. Amani, Design of an S-scheme photo-catalyst utilizing a Cu-doped perovskite and MOF-5 for simultaneous degradation of organic pollutants under LED light irradiation: Application of EXRSM method for spectra separation and BBD-RSM modeling, *Spectrochim. Acta, Part A*, 2023, **287**, 122116.

28 Y.-J. Hao, K.-X. Zhang, M.-Y. Jin, X.-C. Piao, M.-L. Lian and J. Jiang, Improving fed-batch culture efficiency of Rhodiola sachalinensis cells and optimizing flash extraction process of polysaccharides from the cultured cells by BBD–RSM, *Ind. Crops Prod.*, 2023, **196**, 116513.

29 N. I. Madondo and M. Chetty, Anaerobic co-digestion of sewage sludge and bio-based glycerol: Optimisation of process variables using one-factor-at-a-time (OFAT) and Box-Behnken Design (BBD) techniques, *S. Afr. J. Chem. Eng.*, 2022, **40**, 87–99.

30 R. Sanjay, S. Tejeshwini, K. Mamatha and S. Dinesh, Comparative study on structural evaluation of flexible pavement using BBD and FWD, *Mater. Today: Proc.*, 2022, **60**, 608–615.

31 R. Wu, A. S. Abdulhameed, A. H. Jawad, S. K. Yong, H. Li, Z. A. ALOthman, L. D. Wilson and S. Algburi, Development of a chitosan/nanosilica biocomposite with arene functionalization via hydrothermal synthesis for acid red 88 dye removal, *Int. J. Biol. Macromol.*, 2023, **252**, 126342.

32 A. H. Jawad, U. K. Sahu, N. A. Jani, Z. A. ALOthman and L. D. Wilson, Magnetic crosslinked chitosan-tripolyphosphate/MgO/Fe3O4 nanocomposite for reactive blue 19 dye removal: Optimization using desirability function approach, *Surf. Interfaces*, 2022, **28**, 101698.

33 A. S. Abdulhameed, A. H. Jawad, E. Kashi, K. A. Radzun, Z. A. ALOthman and L. D. Wilson, Insight into adsorption mechanism, modeling, and desirability function of crystal violet and methylene blue dyes by microalgae: Box-Behnken design application, *Algal Res.*, 2022, **67**, 102864.

34 A. H. Jawad, A. S. Abdulhameed, S. Surip and S. Sabar, Adsorptive performance of carbon modified chitosan biopolymer for cationic dye removal: kinetic, isotherm, thermodynamic, and mechanism study, *Int. J. Environ. Anal. Chem.*, 2022, **102**, 6189–6203.

35 A. H. Jawad, S. E. M. Saber, A. S. Abdulhameed, A. Reghioua, Z. A. ALOthman and L. D. Wilson, Mesoporous activated carbon from mangosteen (Garcinia mangostana) peels by H3PO4 assisted microwave: Optimization, characterization, and adsorption mechanism for methylene blue dye removal, *Diamond Relat. Mater.*, 2022, **129**, 109389.

36 L. A. Arni, A. Hapiz, A. H. Jawad, A. S. Abdulhameed, Z. A. ALOthman and L. D. Wilson, Fabrication of magnetic chitosan-grafted salicylaldehyde/nanoclay for removal of azo dye: BBD optimization, characterization, and mechanistic study, *Int. J. Biol. Macromol.*, 2023, **248**, 125943.

37 S. Sallam, M. Aljohani, N. M. Alatawi, H. Alsharief, S. F. Ibarhiam, A. Almahri, R. B. Alnoman and N. M. El-Metwaly, Box-Behnken design optimization of bimetallic-organic frameworks for effective removal of tartrazine food dye from aqueous solutions, *J. Mol. Liq.*, 2024, **393**, 123667.

38 P. Bhavyasree and T. Xavier, Adsorption studies of Methylene Blue, Coomassie Brilliant Blue, and Congo Red dyes onto CuO/C nanocomposites synthesized via Vitex negundo Linn leaf extract, *Curr. Res. Green Sustainable Chem.*, 2021, **4**, 100161.

39 H. Wang, H. Xing, K. Yan, D. Han and J. Chen, Oyster shell derived hydroxyapatite microspheres as an effective adsorbent for remediation of Coomassie brilliant blue, *Adv. Powder Technol.*, 2022, **33**, 103425.

40 R. Mallampati, K. S. Tan and S. Valiyaveettil, Utilization of corn fibers and luffa peels for extraction of pollutants from water, *Int. Biodeterior. Biodegrad.*, 2015, **103**, 8–15.

41 J. Divya, K. Palak and P. Vairavel, Optimization, kinetics, equilibrium isotherms, and thermodynamics studies of Coomassie violet dye adsorption using Azadirachta indica (neem) leaf adsorbent, *Desalin. Water Treat.*, 2020, **190**, 353–382.

42 G. Sharma, M. Naushad, A. Kumar, S. Rana, S. Sharma, A. Bhatnagar, F. J. Stadler, A. A. Ghfar and M. R. Khan, Efficient removal of coomassie brilliant blue R-250 dye using starch/poly (alginic acid-cl-acrylamide) nanohydrogel, *Process Saf. Environ. Prot.*, 2017, **109**, 301–310.

43 P. F. de Sales, Z. M. Magriotis, M. A. Rossi, R. F. Resende and C. A. Nunes, Optimization by Response Surface Methodology of the adsorption of Coomassie Blue dye on natural and acid-treated clays, *J. Environ. Manage.*, 2013, **130**, 417–428.

44 M. Abbas, A. Cherfi, S. Kaddour and T. Aksil, Adsorption in simple batch experiments of Coomassie blue G-250 by apricot stone activated carbon—Kinetics and isotherms modelling, *Desalin. Water Treat.*, 2016, **57**, 15037–15048.

45 A. Kadeche, A. Ramdani, M. Adjdir, A. Guendouzi, S. Taleb, M. Kaid and A. Deratani, Preparation, characterization and application of Fe-pillared bentonite to the removal of Coomassie blue dye from aqueous solutions, *Res. Chem. Intermed.*, 2020, **46**, 4985–5008.

46 M. Chauhan, B. Sharma, R. Kumar, G. R. Chaudhary, A. A. Hassan and S. Kumar, Green synthesis of CuO nanomaterials and their proficient use for organic waste removal and antimicrobial application, *Environ. Res.*, 2019, **168**, 85–95.

47 I. Langmuir, The constitution and fundamental properties of solids and liquids. Part I. Solids, *J. Am. Chem. Soc.*, 1916, **38**, 2221–2295.

48 H. M. F. Freundlich, Over the adsorption in solution, *J. Phys. Chem.*, 1906, **57**, 385–471.

49 M. Dubinin, The equation of the characteristic curve of activated charcoal, *Proc. Acad. Sci. USSR, Phys. Chem. Sect.*, 1947, **55**, 327–329.

50 V. P. M. I. Tempkin, Kinetics of ammonia synthesis on promoted iron catalyst, *Acta Physicochim. URSS*, 1940, **12**, 327–356.

51 D. P. Vargas, L. Giraldo and J. C. Moreno-Piraján, CO2 adsorption on activated carbon honeycomb-monoliths: a comparison of Langmuir and Toth models, *Int. J. Mol. Sci.*, 2012, **13**, 8388–8397.

52 S. K. Lagergren, About the theory of so-called adsorption of soluble substances, *Sven. Vetenskapsakad. Handingarl*, 1898, **24**, 1–39.
53 Y.-S. Ho and G. McKay, Sorption of dye from aqueous solution by peat, *Chem. Eng. J.*, 1998, **70**, 115–124.
54 W. J. Weber Jr and J. C. Morris, Kinetics of adsorption on carbon from solution, *J. Sanit. Eng. Div., Am. Soc. Civ. Eng.*, 1963, **89**, 31–59.
55 M. H. Dehghani, A. Dehghan and A. Najafpoor, Removing Reactive Red 120 and 196 using chitosan/zeolite composite from aqueous solutions: Kinetics, isotherms, and process optimization, *J. Ind. Eng. Chem.*, 2017, **51**, 185–195.
56 E. C. Lima, A. Hosseini-Bandegharaei, J. C. Moreno-Pirajᵃn and I. Anastopoulos, A critical review of the estimation of the thermodynamic parameters on adsorption equilibria. Wrong use of equilibrium constant in the Van't Hoof equation for calculation of thermodynamic parameters of adsorption, *J. Mol. Liq.*, 2019, **273**, 425–434.
57 H. N. Tran, S.-J. You, A. Hosseini-Bandegharaei and H.-P. Chao, Mistakes and inconsistencies regarding adsorption of contaminants from aqueous solutions: a critical review, *Water Res.*, 2017, **120**, 88–116.
58 B. Oladipo, E. Govender-Opitz and T. V. Ojumu, Kinetics, thermodynamics, and mechanism of Cu (II) ion sorption by biogenic iron precipitate: using the lens of wastewater treatment to diagnose a typical biohydrometallurgical problem, *ACS Omega*, 2021, **6**, 27984–27993.
59 P. Ilgin and A. Gur, Synthesis and characterization of a new fast swelling poly (EPMA-co-METAC) as superabsorbent polymer for anionic dye absorbent, *Iran. Polym. J.*, 2015, **24**, 149–159.
60 A. H. Jawad, A. S. Abdulhameed, M. M. Hanafiah, Z. A. ALOthman, M. R. Khan and S. Surip, Numerical desirability function for adsorption of methylene blue dye by sulfonated pomegranate peel biochar: modeling, kinetic, isotherm, thermodynamic, and mechanism study, *Korean J. Chem. Eng.*, 2021, **38**, 1499–1509.
61 A. Ivanets, N. Kitikova, I. Shashkova, M. Y. Roshchina, V. Srivastava and M. Sillanpää, Adsorption performance of hydroxyapatite with different crystalline and porous structure towards metal ions in multicomponent solution, *J. Water Proc. Eng.*, 2019, **32**, 100963.
62 S. D. Al-Qahtani, M. Alhasani, N. Alkhathami, K. A. Abu Al-Ola, K. Alkhamis, M. G. El-Desouky and A. A. El-Bindary, Effective levofloxacin adsorption and removal from aqueous solution onto tea waste biochar; synthesis, characterization, adsorption studies, and optimization by Box–Behnken design and its antibacterial activity, *Environ. Technol.*, 2023, **45**(23), 4928–4950.
63 A. Almahri, M. Morad, M. M. Aljohani, N. M. Alatawi, F. A. Saad, H. M. Abumelha, M. G. El-Desouky and A. A. El-Bindary, Atrazine reclamation from an aqueous environment using a ruthenium-based metal-organic framework, *Process Saf. Environ. Prot.*, 2023, **177**, 52–68.
64 T. Musabeygi, N. Goudarzi, M. Mirzaee and M. Arab-Chamjangali, Design of a ternary magnetic composite based on a covalent organic framework and Ag nanoparticles for simultaneous photodegradation of organic pollutants under LED light irradiation: Application of BBD-RSM modeling and resolution of spectral overlap of analytes, *J. Alloys Compd.*, 2023, **964**, 171249.
65 B. Hassan, V. K. Rajan, V. A. Mujeeb and K. Muraleedharan, A DFT based analysis of adsorption of Hg2+ ion on chitosan monomer and its citralidene and salicylidene derivatives: prior to the removal of Hg toxicity, *Int. J. Biol. Macromol.*, 2017, **99**, 549–554.
66 W. Fu and Z. Huang, Magnetic dithiocarbamate functionalized reduced graphene oxide for the removal of Cu (II), Cd (II), Pb (II), and Hg (II) ions from aqueous solution: Synthesis, adsorption, and regeneration, *Chemosphere*, 2018, **209**, 449–456.
67 N. B. Hamadi, A. Guesmi, W. A. El-Fattah, M. A. El-Bindary, M. G. El-Desouky and A. A. El-Bindary, Box–Behnken optimization of stimuli-responsive DOX@Ag-MOF/chitosan — Polycaprolactone nanofiber membranes for smart controlled drug delivery and multifunctional therapeutic applications, *Int. J. Biol. Macromol.*, 2025, **330**, 147989.
68 N. B. Hamadi, A. Guesmi, W. A. El-Fattah, B. H. Alshammari, N. A. Aldawsari, M. G. El-Desouky and A. A. El-Bindary, Design and optimization of chitosan–polyethylenimine encapsulated aluminum–palladium layered double hydroxide for efficient paraquat herbicide adsorption via Box–Behnken approach, *J. Mol. Liq.*, 2025, **437**, 128604.
69 N. A. H. Alshammari, N. H. Elsayed, A. S. Alhawiti, R. A. S. Alatawi, A. A. H. Bukhari, J. S. Alnawmasi, K. B. Alomari, K. M. Alnahdi, H. A. Al-Aoh, M. A. Al-Duais and M. G. El-Desouky, Sustainable nanofibrous cellulose-based hydrogel beads derived from cigarette filter waste, functionalized with hyaluronic acid and encapsulated in chitosan/polyethylenimine for enhanced nickel(II) adsorption from aqueous media, *Int. J. Biol. Macromol.*, 2025, **322**, 146780.
70 A. Guesmi, N. B. Hamadi, W. A. El-Fattah, M. A. El-Bindary, M. G. El-Desouky and A. A. El-Bindary, Sustainable cobalt (II) removal from wastewater using an electrospun Ag-MOF/polycaprolactone-chitosan nanofiber membrane: Optimization and regeneration performance, *Int. J. Biol. Macromol.*, 2025, **319**, 145673.
71 N. B. Hamadi, A. Guesmi, W. A. El-Fattah, T. A. Altalhi, M. A. El-Bindary, M. G. El-Desouky and A. A. El-Bindary, Sustainable removal of Cd(II) using β-Cyclodextrin/Polyethylenimine hydrogel beads embedded with silver-MOFs: Synthesis, characterization, mechanism, and process optimization, *Int. J. Biol. Macromol.*, 2025, **319**, 145663.
72 W. A. El-Fattah, A. Guesmi, N. B. Hamadi, A. Alzahrani, A. A. Alluhaybi and M. G. El-Desouky, Effective of mercury (II) removal from contaminated water using an innovative nanofiber membrane: Kinetics, isotherms, and optimization studies, *Int. J. Biol. Macromol.*, 2025, **311**, 143596.
73 A. Guesmi, N. B. Hamadi, W. A. El-Fattah, A. Subaihi, A. A. Alluhaybi, M. G. El-Desouky and A. A. El-Bindary, Efficient removal of Pb(II) ions from wastewater via

a vanadium metal-organic framework encapsulated with biopolymer carboxymethyl cellulose/polyethylenimine through synthesis, characterization, and Box-Behnken optimization, *Int. J. Biol. Macromol.*, 2025, **318**, 145201.

74 A. Guesmi, N. B. Hamadi, W. A. El-Fattah, A. Subaihi, A. A. Alluhaybi, M. G. El-Desouky and A. A. El-Bindary, Efficient removal of ciprofloxacin in aqueous solutions by magnetic Se-MOF embedded within a biopolymer (chitosan/alginate): Adsorptive behavior, mechanism study, and optimization using Box-Behnken design, *Int. J. Biol. Macromol.*, 2025, **314**, 144274.

75 G. H. Al-Hazmi, L. A. Albedair, A. M. Alsuhaibani, S. H. Alrefaee, I. Althagafi, Q. Mohsen, M. G. El-Desouky, A. A. El-Bindary and K. A. Asla, Synthesis and characterization of functionalized yttrium metal-organic frameworks encapsulated onto bi-polymers for effective removal of As(III); Adsorption isotherms, kinetic, and optimization via Box-Behnken design, *Mater. Today Commun.*, 2025, **45**, 112244.

76 W. A. El-Fattah, A. Guesmi, N. B. Hamadi, M. G. El-Desouky and A. A. El-Bindary, Smart nanocomposite of carbon quantum dots in double hydrogel (carboxymethyl cellulose/chitosan) for effectively adsorb and remove diquat herbicide: Characterization, thermodynamics, isotherms, kinetics, and optimizing through Box-Behnken Design, *Int. J. Biol. Macromol.*, 2025, **309**, 142806.

77 H. S. AlSalem, R. A. S. Alatawi, A. A. H. Bukhari, J. S. Alnawmasi, I. Zghab, M. G. El-Desouky, M. H. Almabadi, Z. H. Alnakhli and N. H. Elsayed, Adsorption and removal of Pb (II) via layer double hydroxide encapsulated with chitosan; synthesis, characterization adsorption isotherms, kinetics, thermodynamics, & optimization via Box-Behnken design, *Int. J. Biol. Macromol.*, 2024, **283**, 137517.

78 S. D. Al-Qahtani, M. Alhasani, N. Alkhathami, K. A. Abu Al-Ola, K. Alkhamis, M. G. El-Desouky and A. A. El-Bindary, Effective levofloxacin adsorption and removal from aqueous solution onto tea waste biochar; synthesis, characterization, adsorption studies, and optimization by Box–Behnken design and its antibacterial activity, *Environ. Technol.*, 2024, **45**, 4928–4950.

79 H. H. Alsharief, N. M. Alatawi, A. M. Al-bonayan, S. H. Alrefaee, F. A. Saad, M. G. El-Desouky and A. A. El-Bindary, Adsorption of Azorubine E122 dye via Na-mordenite with tryptophan composite: batch adsorption, Box–Behnken design optimisation and antibacterial activity, *Environ. Technol.*, 2024, **45**, 3496–3515.

80 A. M. Alsuhaibani, M. S. Refat, A. A. Atta, M. G. El-Desouky and A. A. El-Bindary, Efficient adsorption and removal of tetracycline antibiotics from aqueous solutions onto nickel oxide nanoparticles via organometallic chelate, *Desalin. Water Treat.*, 2022, **277**, 190–205.